mining

MDPI

Article

A Field-Calibrated Physics-Informed Digital Twin Framework for Production Blasting Using Dynamic Finite Element Modeling and Seismic Source Reconstruction

Cemalettin Okay Aksoy [1,*], Guzin Gulsev Uyar Aksoy [2], Hasan Eray Yaman [3], Vehbi Ozacar [3] and Ozan Savas [4]

[1] Mining Engineering Department, Engineering Faculty, Dokuz Eylul University, 35390 Izmir, Turkey
[2] Mining Engineering Department, Engineering Faculty, Hacettepe University, 06800 Ankara, Turkey; gulsevaksoy@hacettepe.edu.tr
[3] Mining Technology Division, Torbali Vocational School, Dokuz Eylul University, 35860 Izmir, Turkey; hasaneray.yaman@deu.edu.tr (H.E.Y.); vehbi.ozacar@deu.edu.tr (V.O.)
[4] GOA Mining Co., 35230 Izmir, Turkey; ozansavas@goamining.com.tr
* Correspondence: okay.aksoy@deu.edu.tr

Abstract

Blast-induced ground vibration is traditionally predicted using empirical scaled-distance equations or numerical simulations driven by simplified analytical loading functions. Although dynamic finite element modeling has significantly advanced the understanding of stress-wave propagation, existing approaches remain unable to reproduce the complete seismic response of actual production blasting because the true blast source is generally unknown and is therefore replaced by simplified pressure–time functions. Consequently, a field-calibrated physics-informed Digital Twin framework for production blasting remains insufficiently established. This study presents a PI-DDT framework for production blasting based on field-derived seismic source reconstruction. The proposed methodology consists of two complementary innovations. First, the three-component near-field pilot-blast record was analyzed through deconvolution-based inverse wave propagation, and the transverse, longitudinal, and vertical components were independently deconvolved to reconstruct three orthogonal equivalent single-hole seismic source histories at the pilot blast hole. Second, the three reconstructed source histories were incorporated into the PLAXIS 3D dynamic finite element model through component-specific dynamic multiplier functions together with the actual production-blast geometry, blast-hole coordinates, electronic initiation sequence, site-specific rock-mass properties, and attenuation characteristics to establish a field-calibrated PI-DDT framework for a full-scale production blast. The proposed framework was applied to a full-scale production blast comprising 83 blast holes in an operating open-pit mine. Model performance was evaluated through a multi-domain performance assessment including PPV, amplitude-envelope development, frequency-spectrum agreement, and cumulative-energy evolution. The simulated responses showed practically meaningful agreement with field measurements across multiple monitoring locations, with a median component PPV error of 11.8%, a mean three-dimensional resultant PPV error of 14.2%, a mean resultant spectral similarity of 84.0%, and a mean three-dimensional cumulative-energy MAE of 4.7%. Unlike conventional blasting simulations that rely on simplified analytical loading functions, the proposed methodology reconstructs a field-derived equivalent seismic source signature and integrates it directly into a physics-based numerical model. The principal scientific contribution of the study lies in the field-calibrated integration of equivalent seismic source reconstruction, actual production-blast geometry and initiation timing, three-dimensional dynamic FEM, and

Check for updates

Academic Editor: Manoj Khandelwal

Received: 18 August 2026
Revised: 12 September 2026
Accepted: 16 September 2026
Published: 28 September 2026

Copyright: © 2026 by the authors. Licensee MDPI, Basel, Switzerland. This article is an open access article distributed under the terms and conditions of the Creative Commons Attribution (CC BY) license.

multi-domain model-performance evaluation within a unified physics-informed framework. The developed framework provides a physics-based computational foundation for blast-design evaluation, vibration-control planning, digital mining applications, and future AI-assisted blast-design optimization and adaptive vibration-control workflows.

Keywords: PI-DDT; production blasting; seismic source reconstruction; inverse wave propagation; dynamic finite element modeling; physics-informed modeling; blast-induced ground vibration; multi-domain model-performance evaluation

1. Introduction

Blast-induced ground vibration remains a major challenge in surface mining, quarrying, tunneling, and large-scale excavation because it directly influences slope stability, nearby infrastructure, environmental compliance, and public acceptance of blasting. Despite substantial advances in drilling, charging, and initiation technologies, vibration prediction is still predominantly based on empirical relationships developed decades ago. These relationships primarily estimate Peak Particle Velocity (PPV), which remains the internationally accepted indicator of blast-induced vibration intensity and structural damage potential [1,2]. However, the integration of field-derived seismic source reconstruction with a physics-based Digital Twin framework for full-scale production blasting remains insufficiently developed.

Peak Particle Velocity (PPV) has become the standard criterion for blast vibration assessment because of its strong correlation with structural response. Accordingly, most predictive equations express PPV as a function of maximum charge per delay and scaled distance.

$$\mathrm{PPV} = \mathrm{K}\left(\frac{R}{\sqrt{W}}\right)^{-n} \quad (1)$$

where PPV is the Peak Particle Velocity, K is the site constant, n is the attenuation exponent, R is the distance between the blast and the monitoring location, and W is the maximum charge per delay. The scaled distance is defined as $\mathrm{SD} = \mathrm{R}/\sqrt{W}$.

Although these empirical equations are computationally efficient, they reduce the complex physics of blasting to a simple attenuation relationship. In reality, blast-induced seismic wave propagation is controlled by multiple interacting processes, including explosive energy release, wave propagation, attenuation, geological heterogeneity, and delay-sequence interference, none of which are explicitly represented in conventional scaled-distance formulations (Figure 1).

Classical blast vibration prediction has traditionally relied on empirical scaled-distance relationships that correlate PPV with explosive charge weight and distance [1–5]. Although these formulations remain widely used because of their simplicity, they reduce blast-induced vibration to a site-dependent attenuation relationship and cannot explicitly represent explosive–rock interaction, initiation timing, wave interference, frequency content, or geological heterogeneity.

To improve prediction accuracy, numerous statistical and machine-learning approaches have been proposed, including artificial neural networks, support vector machines, fuzzy inference systems, random forests, and hybrid optimization algorithms [6–11]. While these methods often outperform empirical equations within calibrated datasets, they remain largely data-driven and site-specific, providing limited physical insight into seismic-wave generation and propagation.

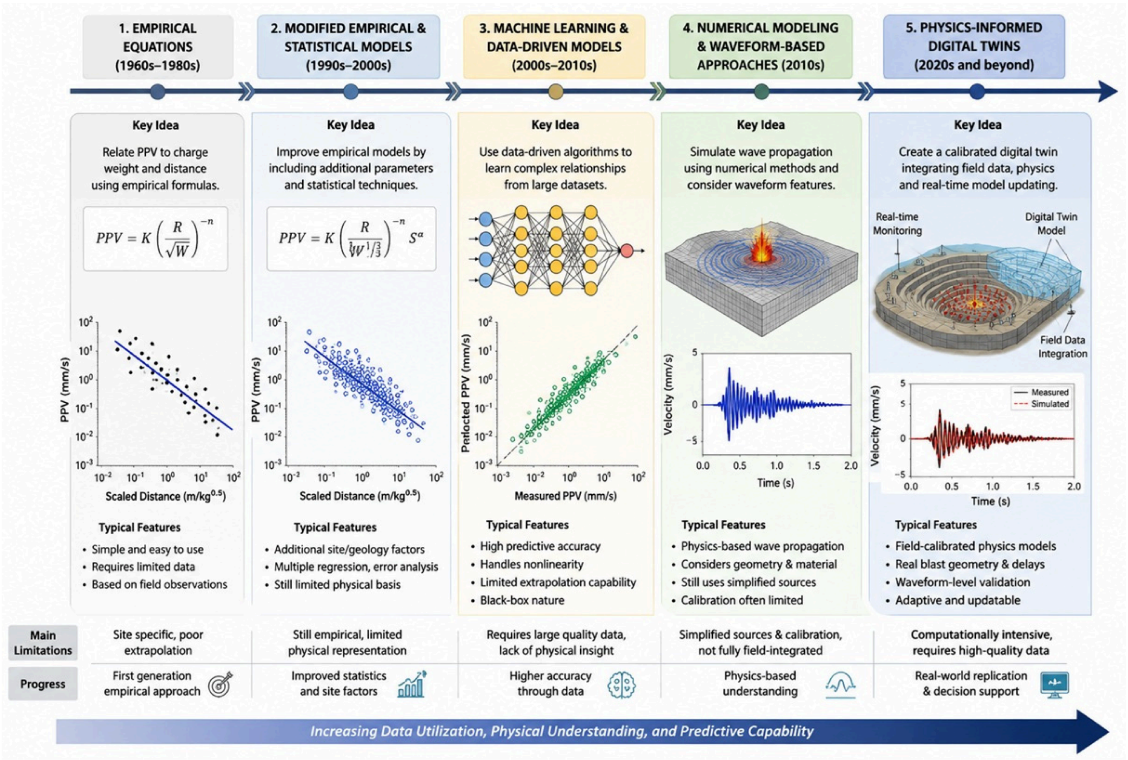


Figure 1. Evolution of blast vibration prediction methodologies from empirical equations to physics-informed digital twins.

Experimental studies further demonstrate that only a fraction of the explosive energy is converted into seismic waves, whereas most of the energy is consumed by fragmentation, crack propagation, gas expansion, and rock deformation [12–15]. Consequently, simplified analytical loading functions cannot realistically represent the field-recorded seismic source of production blasting.

Dynamic numerical methods, including FEM, FDM, DEM, and coupled continuum–discontinuum approaches, provide a rigorous framework for simulating stress-wave propagation and blast-induced rock response [16–21]. Nevertheless, most existing simulations still employ idealized pressure pulses or analytical source functions, limiting their ability to reproduce measured waveforms, frequency-dependent attenuation, and delay-induced wave interference. Consequently, a clear methodological gap remains in integrating field-derived seismic source reconstruction with a Physics-Informed Dynamic Digital Twin framework for real production blasting.

$$M\ddot{u}(t) + \dot{C}\ddot{u}(t) + K_u(t) = F(t) \quad (2)$$

where M, C and K denote the global mass, damping and stiffness matrices, respectively; u is the nodal displacement vector; and F(t) denotes the generalized external dynamic excitation term in the governing elastodynamic equation. In the present FEM implementation, the reconstructed field-derived source histories were introduced into the PLAXIS 3D model through component-specific dynamic multiplier functions, as described in Section 2.5.

However, despite the mathematical sophistication of these numerical methods, a fundamental limitation remains unresolved. The principal differences between conventional blast-vibration prediction approaches and the proposed field-calibrated PI-DDT framework are summarized in Table 1.

Table 1. Comparison between conventional blast vibration prediction approaches and the proposed field-calibrated PI-DDT framework.

Feature	Empirical Models	Machine-Learning Models	Conventional Numerical Models	Proposed Field-Calibrated PI-DDT Framework
Primary objective	PPV prediction	PPV prediction/pattern recognition	Wave-propagation simulation	Field-calibrated production-blast representation
Physical basis	Empirical attenuation	Data-driven correlations	Physics-based numerical mechanics	Physics-informed and field-calibrated dynamic modeling
Seismic source	Not explicitly represented	Implicit in training data	Usually idealized pressure–time function	Field-derived equivalent seismic source reconstructed from pilot-blast records
Blast geometry	Simplified distance/charge terms	Usually not represented explicitly	Partially or ideally represented	Actual production-blast geometry and blast-hole coordinates
Electronic initiation sequence	Indirectly represented	Implicit or absent	Often simplified	Actual field electronic initiation times applied hole-by-hole
Rock-mass characterization	Site constants	Implicit in data	Engineering material parameters	Site-specific effective rock-mass properties
Attenuation treatment	Empirical decay coefficients	Implicit in training data	Material damping/boundary damping	Effective field-scale Q and damping calibrated in forward model
Performance-evaluation criterion	Mostly PPV	Mostly PPV or prediction error	Often PPV and selected waveforms	PPV, resultant PPV, envelope, spectrum, and cumulative energy
Digital Twin capability	No	No	No	Event-based, field-calibrated PI-DDT framework/prototype
Continuous updating using field data	No	Possible if designed	Generally no	Future implementation
AI-assisted optimization compatibility	Limited	Moderate	Limited to coupled workflows	Framework-compatible; future capability
Engineering use	Regulatory vibration estimation	Site-specific prediction	Scenario simulation	Blast-design evaluation, vibration-control planning, and scenario analysis

Previous studies demonstrated that blast-induced vibration can be reduced by optimizing delay timing and promoting destructive wave interference [22–26]. However, these investigations focused primarily on waveform analysis and vibration mitigation rather than constructing a physics-based three-dimensional numerical replica of a real production blast.

Consequently, a critical gap remains between field-recorded seismic measurements and physics-based numerical simulation. Existing approaches have not integrated field-derived seismic source reconstruction, actual blast-hole geometry, real electronic initiation sequences, calibrated attenuation characteristics, and multi-domain model-performance evaluation within a single dynamic finite element framework. Furthermore, the original seismic source generated at the blast hole is almost always replaced by simplified analytical

loading functions, limiting the physical realism of numerical simulations and preventing the development of a truly field-calibrated Digital Twin.

To address this limitation, the present study reconstructs the seismic source rather than prescribing it. The three-component near-field pilot-blast record is processed using deconvolution-based inverse wave propagation, with the transverse, longitudinal, and vertical components independently deconvolved to reconstruct three orthogonal equivalent single-hole seismic source histories at the blast hole. The reconstructed equivalent source signature is then introduced into a three-dimensional dynamic finite element model as field-derived dynamic excitation, preserving the principal temporal and spectral characteristics required for forward wave-propagation analysis.

Recent advances in sensing technologies, computational mechanics, and high-performance computing have accelerated the adoption of Digital Twin concepts across engineering disciplines [27–32]. Although Digital Twins have been applied to equipment monitoring, autonomous mining, slope stability, ventilation, and underground construction, production blasting has remained one of the least digitally replicated mining operations despite its critical influence on fragmentation, vibration, and slope response.

Accordingly, this study develops a PI-DDT for production blasting by integrating field-recorded pilot-blast waveforms, deconvolution-based seismic source reconstruction, actual blast-hole coordinates, real electronic initiation sequences, site-specific rock-mass properties, frequency-dependent attenuation, and three-dimensional dynamic finite element modeling. Unlike conventional PPV-only assessments, the proposed framework is evaluated using multiple complementary response domains, including PPV, amplitude-envelope development, frequency-spectrum agreement, and cumulative-energy evolution, thereby establishing a field-calibrated physics-informed numerical representation of the production-blast response.

As summarized in Figure 2 and Table 2, empirical, data-driven, and conventional numerical approaches each exhibit important limitations. None simultaneously combines field-derived source reconstruction, physics-based three-dimensional modeling, actual production-blast geometry, and comprehensive multi-domain model-performance evaluation within a unified Digital Twin framework, representing the principal scientific contribution of the present study.

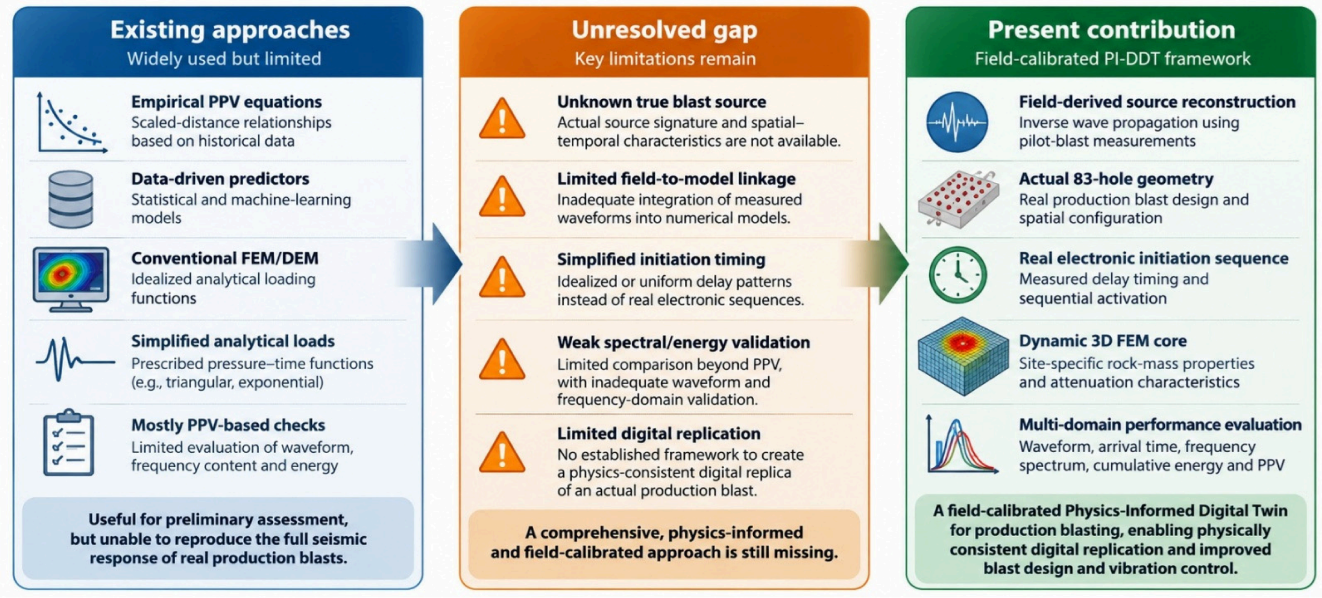


Figure 2. Research gap in existing blast vibration prediction approaches and the scientific contribution of the proposed PI-DDT framework.

Table 2. Key scientific contributions introduced by the proposed PI-DDT framework.

Contribution	Engineering Significance
Field-derived equivalent seismic source	Preserves the temporal and spectral characteristics of a measured pilot-blast response and provides a physically grounded input for dynamic FEM.
Deconvolution-based inverse source reconstruction	Estimates an equivalent single-hole seismic source by correcting the near-field pilot-blast record for geometric spreading and travel-time phase delay.
Waveform-driven dynamic finite element model	Uses a field-derived source history rather than an assumed analytical pressure–time pulse for production-blast wave-propagation analysis.
Actual production-blast geometry	Incorporates the 83-hole blast geometry and field coordinates into the numerical representation.
Real electronic initiation timing	Applies the measured electronic initiation sequence hole-by-hole instead of using simultaneous or idealized delay activation.
Full-scale production-blast implementation	Demonstrates the framework on an operating open-pit production blast under field conditions.
Multi-domain model-performance evaluation	Assesses the model using PPV, resultant PPV, amplitude-envelope development, spectral similarity, and cumulative-energy evolution.
Event-based field-calibrated PI-DDT framework	Defines a physics-informed virtual representation of the production-blast process linked to field-derived source, geometry, timing, parameters, and monitoring responses.
Foundation for future adaptive blasting workflows	Provides a computational basis for future scenario analysis, uncertainty-aware model updating, and AI-assisted blast-design optimization.

Figure 2 illustrates the evolution of blast vibration prediction from empirical attenuation models to a PI-DDT. Unlike conventional approaches, the proposed framework integrates field-derived seismic sources, realistic blast geometry, three-dimensional dynamic finite element modeling, and comprehensive multi-domain model-performance evaluation, thereby establishing a field-calibrated physics-informed numerical representation of an actual production blast rather than a conventional vibration-prediction model.

Another important limitation of previous studies is their reliance on Peak Particle Velocity (PPV) as the primary model-performance criterion. Although PPV is the internationally accepted engineering index for blast vibration assessment [1,2], it represents only the maximum amplitude of a transient signal and cannot fully characterize waveform evolution, frequency content, or energy distribution. As summarized in Figure 2 and Table 2, no existing methodology simultaneously combines field-recorded seismic sources, realistic blast geometry, electronic initiation sequences, physics-based dynamic simulation, and multi-domain model-performance evaluation within a unified Digital Twin framework.

To address this gap, the present study develops a PI-DDT by integrating field-recorded pilot-blast waveforms, deconvolution-based inverse wave propagation, actual production-blast geometry, real electronic initiation sequences, site-specific rock-mass properties, frequency-dependent attenuation, and three-dimensional dynamic finite element modeling. The conceptual architecture of the proposed framework is presented in Figure 3, comprising four interconnected components: (i) field measurements, (ii) seismic source reconstruction, (iii) waveform-driven three-dimensional dynamic FEM, and (iv) field-to-model synchronization and multi-domain performance evaluation. Event-based comparison between

measured and simulated responses provides the field-calibration link between the physical production blast and its physics-informed numerical counterpart.

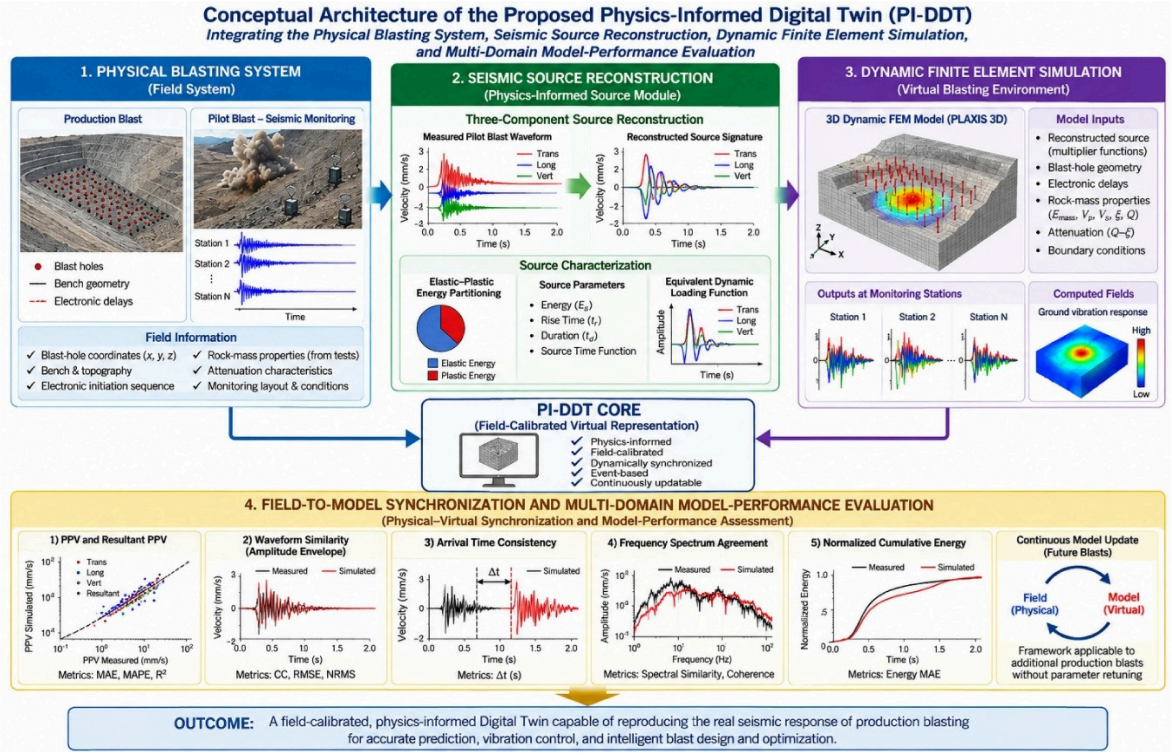


Figure 3. Conceptual architecture of the proposed PI-DDT integrating the physical blasting system, seismic source reconstruction, dynamic finite element simulation, and multi-domain model-performance evaluation.

The practical implementation of the proposed framework is summarized in Figure 4. The three-component near-field pilot-blast record is first processed through deconvolution-based inverse wave propagation, with the transverse, longitudinal, and vertical components independently deconvolved to reconstruct three orthogonal equivalent single-hole seismic source histories. The reconstructed equivalent source representation is then incorporated into a three-dimensional dynamic finite element model together with the actual blast geometry, electronic initiation sequence, site-specific rock-mass properties, and attenuation characteristics. Finally, the simulated and measured responses are compared through multi-domain model-performance evaluation to establish the field-calibration link between the production blast and its physics-informed numerical counterpart.

The proposed methodology is demonstrated through a full-scale production blast involving 83 blast holes initiated using the actual electronic delay sequence. The novelty of the proposed framework lies in the integration of field-derived seismic source reconstruction, three-dimensional dynamic finite element modeling, actual blast geometry, site-specific material properties, and multi-domain model-performance evaluation within a single PI-DDT framework. This framework transforms blast vibration analysis from empirical prediction into physics-based digital replication, providing a foundation for intelligent blast design, adaptive vibration control, and future AI-assisted blasting systems.

Accordingly, this study aims to: (1) develop a PI-DDT for production blasting; (2) reconstruct an equivalent single-hole seismic source signature through deconvolution-based inverse wave propagation and incorporate the resulting field-derived excitation into a three-dimensional dynamic finite element model; (3) evaluate the PI-DDT performance using PPV-, amplitude-envelope-, spectral-, and energy-based indicators and

(4) demonstrate a physics-informed computational framework for realistic digital replication of production blasting.

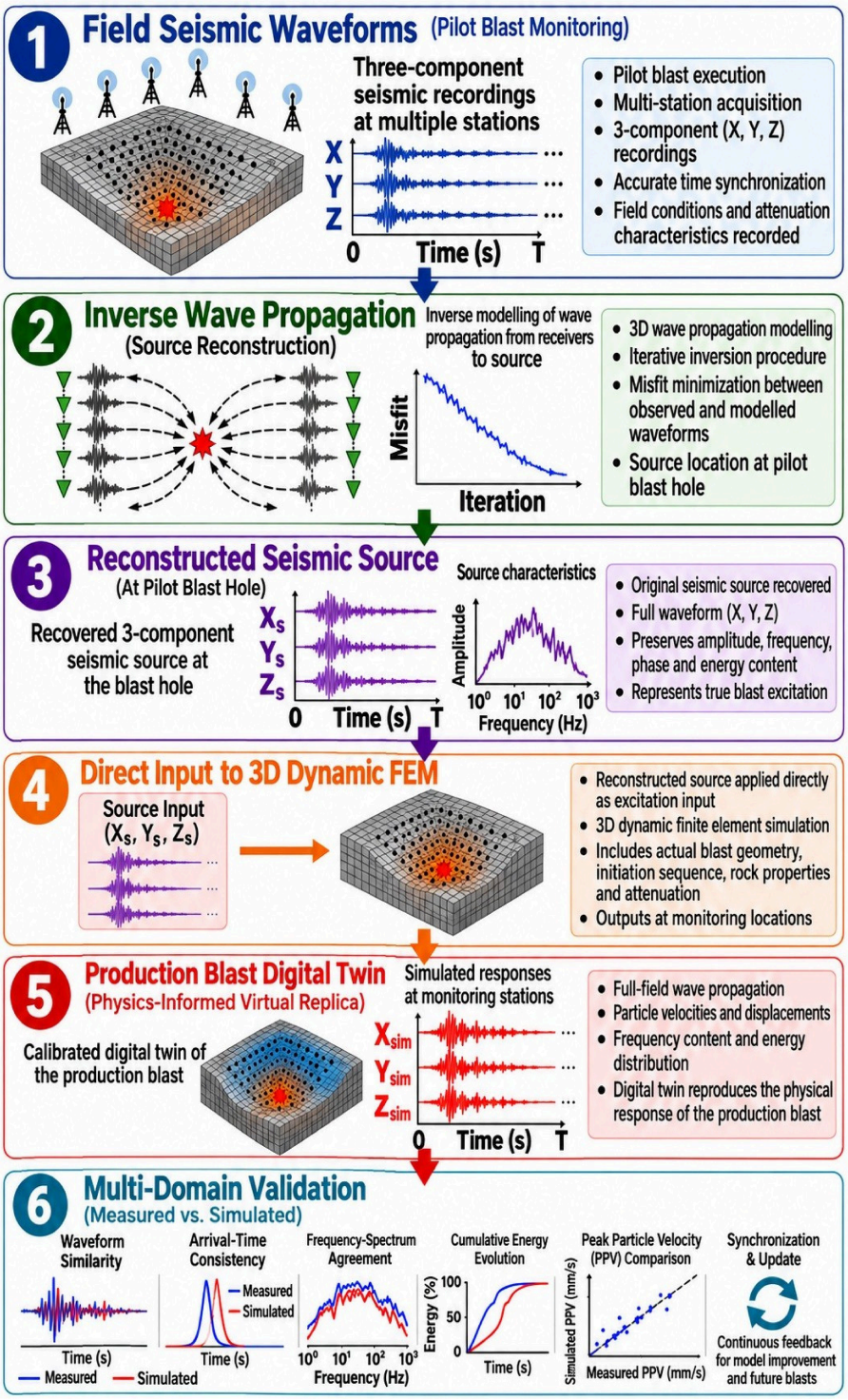


Figure 4. Overall workflow of the proposed PI-DDT integrating field measurements, source reconstruction, three-dimensional finite element modeling, and multi-domain model-performance evaluation of production blasting.

The proposed methodology fundamentally changes the role of numerical modeling in blasting engineering by transforming field observations into a field-calibrated, physics-informed virtual representation of an actual production blast rather than a conventional vibration prediction model. As summarized in Table 2, the proposed framework integrates

field-derived seismic source reconstruction, three-dimensional dynamic finite element modeling, actual blast geometry, and comprehensive multi-domain model-performance evaluation within a unified Digital Twin architecture. Collectively, these integrations establish a physics-informed framework capable of reproducing the principal amplitude, spectral, and energy characteristics of the monitored production-blast response.

As summarized in Table 2, the novelty of the present study lies not in the individual methodologies but in their integration within a unified PI-DDT. Accordingly, the scientific contribution lies in combining field-derived seismic source reconstruction, inverse wave propagation, three-dimensional dynamic finite element modeling, actual production-blast geometry and timing, and multi-domain model-performance evaluation within a unified computational framework.

2. Materials and Methods

The methodology developed in this study integrates field measurements, seismic source reconstruction, and three-dimensional dynamic finite element modeling within a unified Physics-Informed Dynamic Digital Twin (PI-DDT) framework. This section describes the overall methodological architecture and the principal components used to construct, synchronize, and evaluate the field-calibrated PI-DDT representation of the production blast.

2.1. PI-DDT Methodological Framework

The proposed PI-DDT establishes a dynamically synchronized virtual representation of a real production blast by integrating field observations with three-dimensional dynamic finite element modeling. Unlike conventional blasting analyses based on empirical attenuation relationships or simplified loading functions, the proposed framework reconstructs the seismic source from field measurements and directly applies it to a calibrated numerical model, enabling realistic simulation of blast-induced seismic wave propagation. The overall methodological workflow is presented in Figure 5 and consists of six sequential stages: (i) field acquisition of pilot- and production-blast data, (ii) deconvolution-based inverse wave propagation for seismic source reconstruction, (iii) construction of a three-dimensional dynamic finite element model, (iv) direct application of the reconstructed seismic source together with the actual electronic initiation sequence, (v) simulation of the complete production blast, and (vi) field-to-model synchronization and multi-domain performance evaluation using measured production-blast responses.

The workflow begins with acquisition of three-component seismic waveforms from a pilot blast together with production-blast geometry, blast-hole coordinates, electronic initiation sequences, explosive distribution, and site-specific rock-mass properties. These data provide the physical basis for Digital Twin construction. The three near-field pilot-blast components are subsequently processed independently through deconvolution-based inverse wave propagation to reconstruct orthogonal equivalent single-hole seismic source histories retaining the principal temporal and spectral characteristics required for forward dynamic analysis. The reconstructed three-component source histories are then introduced into the PLAXIS 3D dynamic finite element model through component-specific dynamic multiplier functions representing the field-derived excitation of the production blast.

Finally, simulated and measured responses are compared through multi-domain model-performance evaluation using PPV, amplitude-envelope development, frequency-spectrum similarity, and normalized cumulative-energy evolution. Consequently, the developed PI-DDT enables the production-blast response to be evaluated across complementary amplitude, temporal-envelope, spectral, and energy domains.

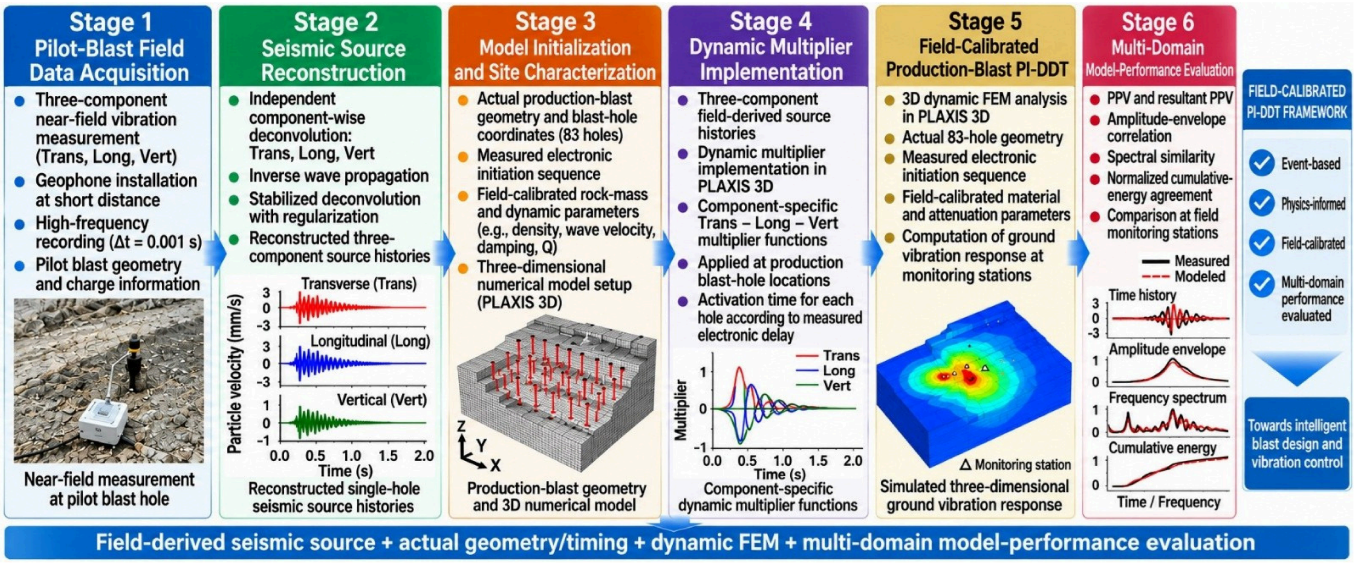


Figure 5. Overall methodological framework of the proposed PI-DDT.

2.2. Field Data Acquisition

The proposed PI-DDT was developed entirely from field-derived measurements acquired under actual operating conditions. The field campaign comprised two complementary stages: (i) a pilot blast for seismic source reconstruction and (ii) a full-scale production blast consisting of 83 blast holes initiated using the actual electronic delay sequence for PI-DDT implementation, calibration, and model-performance evaluation.

The overall field measurement strategy is illustrated in Figure 6. The acquired dataset included both the physical characteristics of the blasting system and the corresponding seismic response. Geometric and operational data comprised blast-hole coordinates, burden, spacing, bench geometry, hole depth, explosive distribution, and electronic initiation timing, while three-component seismic waveforms were simultaneously recorded at multiple monitoring stations surrounding the production blast.

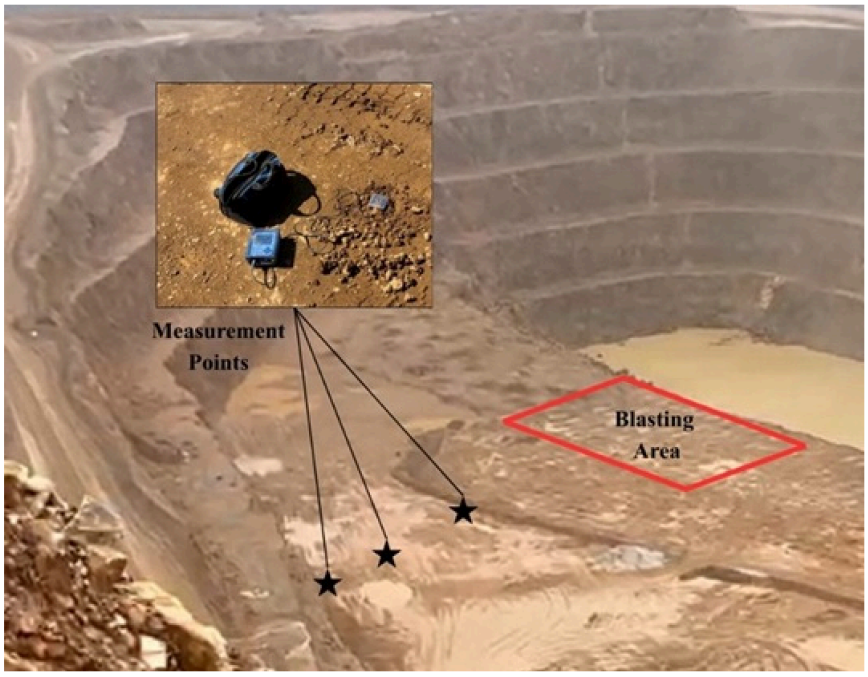


Figure 6. Field data acquisition strategy adopted for the development of the proposed PI-DDT.

The field measurements served two complementary purposes. Geometric and blasting parameters were incorporated directly into the three-dimensional dynamic finite element model, whereas the recorded pilot-blast waveforms provided the input for deconvolution-based inverse wave propagation and seismic source reconstruction. The principal field measurements are summarized in Table 3.

Table 3. Field monitoring records used for production-blast model calibration and performance evaluation.

Monitoring Point	Distance (m)	Measured PPV Transverse (mm/s)	Measured PPV Longitudinal (mm/s)	Measured PPV Vertical (mm/s)	Role in Manuscript
UM24232	22	17.08	33.35	32.49	Production-blast monitoring/model-performance evaluation
12269	28	12.70	27.05	12.57	Production-blast monitoring/model-performance evaluation
UM6761	34	11.48	33.66	15.67	Production-blast monitoring/model-performance evaluation

Because both seismic source reconstruction and numerical simulation originate from the same field observations, the resulting PI-DDT maintains direct physical consistency with the actual production blasting system and provides the field basis for subsequent multi-domain model-performance evaluation.

2.3. Field Seismic Source Reconstruction by Deconvolution-Based Inverse Wave Propagation

The principal methodological component of this study is the reconstruction of an equivalent single-hole seismic source signature directly from the field-recorded response of the pilot blast. Unlike conventional blasting simulations, in which the dynamic excitation is commonly prescribed using an idealized analytical pressure–time function, the present approach derives the numerical excitation from a field-measured seismic response. The objective of the inverse procedure is therefore not to recover the explosive detonation pressure history itself, but to estimate an equivalent seismic source signature at the pilot blast hole that retains the principal dynamic characteristics transmitted from the single-hole blast into the surrounding rock mass.

For a pilot blast recorded at monitoring location j, the measured particle-velocity waveform can be represented by the source–path–receiver relationship:

$$v_{\{j\}}(t) = \mathrm{s}(t) \times h_j(t) + n_j(t) \quad (3)$$

where $v_j(t)$ is the measured particle-velocity time history at monitoring location j, s(t) is the unknown equivalent single-hole seismic source signature at the pilot blast hole, $h_j(t)$ is the propagation response between the source and receiver, $n_j(t)$ represents measurement noise and unmodeled local effects, and * denotes convolution. Equation (3) provides the physical basis of the inverse reconstruction: the field-recorded waveform contains both the dynamic characteristics of the blast-generated source and the modifications introduced during propagation through the rock mass. The inverse procedure therefore seeks to compensate for the principal propagation effects and recover an equivalent source signature at the blast-hole location.

Applying the Fourier transform to Equation (3) converts convolution in the time domain into multiplication in the frequency domain:

$$V_{\{j\}(\omega)} = \mathrm{S}(\omega) H_{j(\omega)} + N_{\{j\}(\omega)} \tag{4}$$

where $\mathrm{V_j}(\omega)$, $\mathrm{S}(\omega)$, $\mathrm{H_j}(\omega)$, and $\mathrm{N_j}(\omega)$ are the Fourier transforms of the measured waveform, equivalent source signature, propagation transfer function, and noise contribution, respectively. Neglecting the noise term in the first-order inverse formulation, the source spectrum can formally be estimated by spectral deconvolution:

$$S_{j(\omega)} = \frac{V_{j(\omega)}}{H_{j(\omega)}} \tag{5}$$

Direct spectral division may become unstable at frequencies for which $|\mathrm{H_j}(\omega)|$ is small and may consequently amplify measurement noise. A stabilized deconvolution scheme was therefore adopted:

$$\hat{S}(\omega) = [V_j(\omega)\, H_j{}^*(\omega)]/[\,|H_j(\omega)|^2 + \lambda] \tag{6}$$

where $H_j{}^*(\omega)$ denotes the complex conjugate of the transfer function and λ is the regularization parameter:

$$\lambda = 0.01\ max(|H_j(\omega)|^2) \tag{7}$$

The adopted value corresponds to a 1% regularization threshold relative to the maximum squared amplitude of the transfer function. This regularization suppresses numerical amplification near spectral minima while retaining the usable frequency content of the recorded pilot-blast signal. The procedure stabilizes the inverse filtering without replacing the measured source characteristics with an assumed analytical excitation.

The monitoring record used for source reconstruction was acquired in the immediate near field of the single-hole pilot blast, at a source–receiver distance of approximately 10 m. Over this short propagation path, the inverse reconstruction considered spherical geometric spreading and propagation-time phase delay. Intrinsic anelastic attenuation was not explicitly included in the source-inversion transfer function. Accordingly, the transfer function was expressed as:

$$H_j(\omega) = (1/r_j)\ exp[-i\omega(r_j/V_p)] \tag{8}$$

where $\mathrm{r_j}$ is the source–receiver distance and $\mathrm{V_p}$ is the in situ P-wave velocity used to determine the propagation-time correction. The corresponding travel time is:

$$\tau_j = r_j/V_p \tag{9}$$

The $1/\mathrm{r_j}$ term in Equation (8) represents spherical body-wave geometric spreading, whereas the exponential term represents the phase shift associated with the propagation time from the pilot blast hole to the monitoring location. Importantly, $\mathrm{V_p}$ was not prescribed arbitrarily and was not selected from Table 3. It was automatically determined by the seismic-processing software from the recorded pilot-blast seismic waveform and subsequently used in the travel-time correction applied during source reconstruction. Thus, Table 3 is not the source of the $\mathrm{V_p}$ value employed in Equations (8) and (9).

Because the pilot source–receiver distance was only approximately 10 m, intrinsic anelastic attenuation was deliberately omitted from the inverse source-reconstruction stage. In particular, the seismic quality factor Q and the damping ratio used subsequently in the forward finite element simulations were not used to reconstruct the seismic source. This

distinction separates the near-field source inversion from the attenuation and damping treatment employed in the forward dynamic FEM.

A sensitivity analysis was performed to assess the influence of the regularization parameter on the reconstructed source and subsequent model response. The regularization threshold was varied from 0.5% to 5% of max $|H_j(\omega)|^2$, while the adopted value of 1% was retained as the reference case. Because the transfer function used in the present near-field reconstruction has a frequency-independent magnitude, $|H(\omega)| = 1/r$, variation of the regularization threshold primarily produces a uniform scaling of the reconstructed source amplitude without modifying its normalized spectral shape or phase characteristics. Relative to the 1% reference case, the reconstructed-source amplitude varied by approximately +0.5% to −3.8% over the investigated range. The corresponding mean component-level PPV error ranged from 12.67% to 15.21%, while the mean three-dimensional resultant PPV error ranged from 12.39% to 14.43%. The normalized spectral and cumulative-energy characteristics remained unchanged under this positive scalar rescaling. These results demonstrate that the adopted 1% regularization threshold provides a stable reconstruction and that the principal conclusions of the study are not sensitive to moderate variations in λ. Additional details of the regularization-parameter sensitivity analysis are provided in Section S1 of the Supplementary Materials.

Three-component particle-velocity measurements were available from the near-field pilot-blast monitoring record, and the inverse reconstruction was performed independently for the transverse, longitudinal, and vertical components. Each component was transformed into the frequency domain and deconvolved separately using the stabilized inverse formulation defined in Equations (6)–(8). The corresponding component-wise source spectra were then transformed back into the time domain to obtain three orthogonal equivalent single-hole seismic source histories. These reconstructed transverse, longitudinal, and vertical source histories were subsequently used to define three component-specific dynamic multiplier functions implemented in the forward PLAXIS 3D model.

Accordingly, the source-reconstruction sequence can be summarized as:

$$v_k(t) \xrightarrow{\mathcal{F}} V_k(w) \overset{deconvolution}{\rightarrow} \hat{S}_k(w) = \frac{V_k(w)H_k^*(w)}{|H_k(w)|^2 + \lambda} \xrightarrow{\mathcal{F}^{-1}} \hat{s_k}(t), \quad k \in \{Trans,\ Long,\ Vert\} \tag{10}$$

where $v_k(t)$ denotes the measured near-field pilot-blast particle-velocity history for component k, $V_k(w)$ is its Fourier spectrum, $H_k(w)$ is the corresponding near-field propagation transfer function, $\hat{S}_k(w)$ is the stabilized reconstructed source spectrum, and $\hat{s_k}(t)$ is the reconstructed time-domain equivalent single-hole seismic source history. The index k represents the transverse, longitudinal, and vertical components, each of which was processed independently through the same deconvolution procedure. The final time-domain signature was obtained by inverse Fourier transformation:

$$\hat{s_k}(t) = F^{-1}\left[\hat{S}(\omega)\right] \quad k \in \{Trans,\ Long,\ Vert\} \tag{1}$$

The reconstructed $\hat{s_k}(t)$ histories therefore represent the three field-derived orthogonal components of the equivalent single-hole seismic source after compensation for the principal near-field propagation effects included in the inverse model. These histories should be interpreted collectively as a three-component equivalent seismic source representation for subsequent dynamic numerical analysis rather than as the explosive detonation pressure–time history itself.

The deconvolution-based reconstruction workflow is illustrated in Figure 7. The procedure begins with the three-component near-field seismic record of the single-hole pilot blast. The transverse, longitudinal, and vertical components are transformed independently into the frequency domain, corrected using the corresponding near-field propagation transfer

function, and subjected separately to stabilized deconvolution using the 1% regularization threshold defined in Equation (7). The three reconstructed source spectra are then transformed back into the time domain to obtain the orthogonal equivalent single-hole seismic source histories.

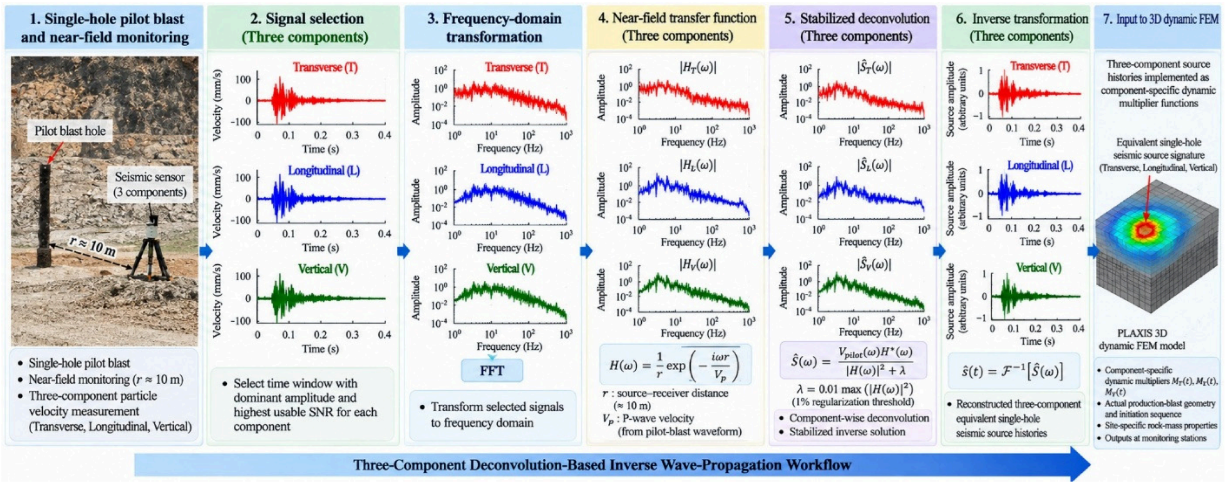
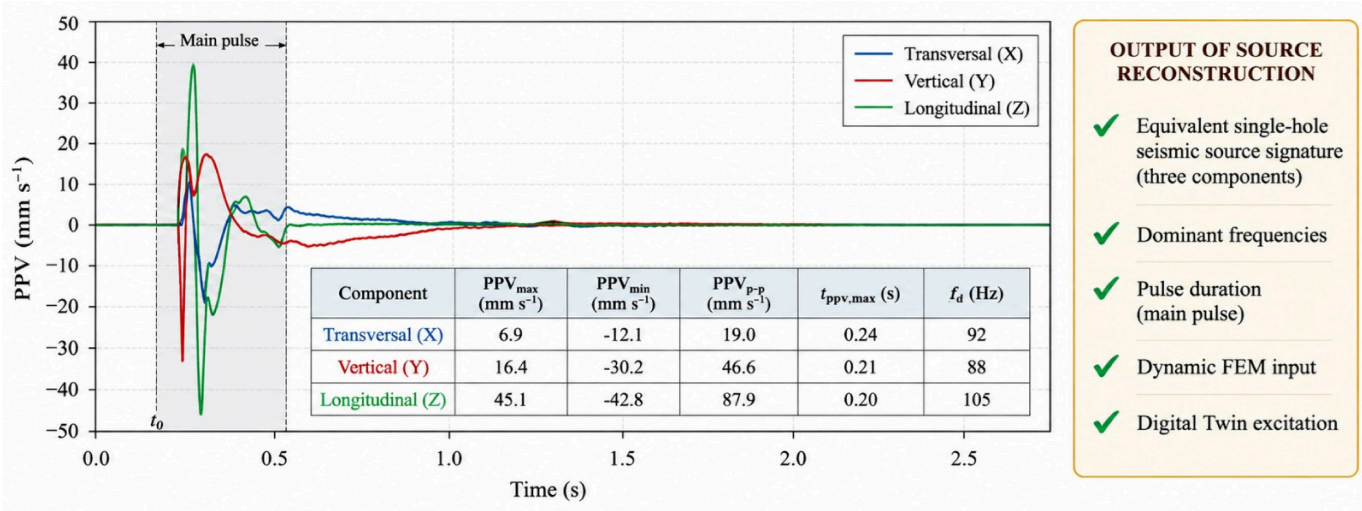


Figure 7. Deconvolution-based inverse wave-propagation workflow used to reconstruct the three orthogonal equivalent single-hole seismic source histories from the near-field pilot-blast record. The transverse, longitudinal, and vertical components were transformed independently into the frequency domain, corrected for spherical geometric spreading and travel-time phase delay, and subjected separately to stabilized deconvolution using the 1% regularization threshold defined in Equation (7) before inverse Fourier transformation.

The reconstructed three-component source histories were subsequently used to define the field-derived dynamic multiplier functions implemented in the three-dimensional PLAXIS 3D model. As shown in Figure 8, the reconstructed equivalent single-hole seismic source signature retains the principal temporal and spectral characteristics of the pilot-blast seismic response after correction for the propagation effects represented in the inverse model. Unlike an assumed analytical pressure–time pulse, this field-derived signature provides a physically grounded excitation for the subsequent dynamic simulation. Its implementation in the production-blast FEM, together with the actual blast-hole locations and electronic initiation sequence, is described in Sections 2.4 and 2.5.

As a component-wise numerical illustration of the reconstruction procedure, each measured near-field particle-velocity component was processed independently according to Equations (6)–(11). For a given component k, the measured spectrum $V_k(\omega)$ was corrected using the corresponding near-field transfer function $H_k(\omega)$, and the stabilized reconstructed spectrum $\hat{S}_k(\omega)$ was obtained using the 1% regularization threshold defined in Equation (7). Inverse Fourier transformation then yielded the corresponding time-domain source history $\hat{s_k}(t)$. Applying this procedure independently to the transverse, longitudinal, and vertical records produced the three reconstructed source histories presented in Figure 8. The reconstructed histories preserve the component-specific pulse duration, dominant-frequency content, waveform morphology, and relative amplitude evolution of the field-derived excitation, thereby providing a numerical reconstruction example of the complete frequency-domain-to-time-domain inverse procedure.

The inverse reconstruction was performed independently for the transverse, longitudinal, and vertical near-field components, and the resulting three orthogonal source histories were subsequently used to define the component-specific dynamic multiplier functions implemented in the forward PLAXIS 3D model, as described in Section 2.5.



Component	PPV_{max} (mm s^{-1})	PPV_{min} (mm s^{-1})	PPV_{p-p} (mm s^{-1})	$t_{ppv,max}$ (s)	f_d (Hz)
Transversal (X)	6.9	-12.1	19.0	0.24	92
Vertical (Y)	16.4	-30.2	46.6	0.21	88
Longitudinal (Z)	45.1	-42.8	87.9	0.20	105

Figure 8. Component-wise numerical reconstruction example showing the three-component equivalent single-hole seismic source signature obtained from the near-field pilot-blast record through deconvolution-based inverse wave-propagation analysis. The transverse, longitudinal, and vertical source histories were reconstructed independently according to Equations (6)–(11) and subsequently used to define the three orthogonal field-derived dynamic multiplier functions implemented in the PLAXIS 3D model.

The reconstructed equivalent source representation retains the principal temporal and spectral characteristics required for the subsequent numerical analysis, including pulse duration, dominant frequency content, waveform morphology, and relative amplitude evolution. This field-derived source representation provides the physical link between the pilot-blast measurement and the forward dynamic simulation used in the proposed PI-DDT framework.

2.4. Three-Dimensional Dynamic Finite Element Model and Digital Twin Construction

Following reconstruction of the field-derived equivalent single-hole seismic source signature, a three-dimensional dynamic finite element (FEM) model was developed as the computational core of the proposed PI-DDT framework. The model incorporated the reconstructed source signature together with the actual production-blast geometry, blast-hole coordinates, electronic initiation sequence, and site-specific rock-mass properties, thereby providing a field-informed numerical representation of blast-induced seismic-wave propagation.

The computational domain had overall dimensions of 850 m × 460 m × 300 m and was discretized using three-dimensional solid finite elements. The generated mesh comprised 5581 elements and 9161 nodes. Because the model contains geometrically and dynamically different regions, a non-uniform mesh was adopted. The resulting element sizes ranged from 0.9029 m to 128.1 m, with an average element size of 52.23 m. The mesh-generation settings included a global scale factor of 1.2 and a minimum element-size factor of 0.005. These parameters are reported explicitly to improve reproducibility of the numerical model.

For transient wave-propagation analysis, spatial discretization must be sufficiently fine relative to the wavelengths represented by the dynamic excitation. The characteristic mesh requirement was expressed as:

$$h \leq \frac{\lambda_{\{min\}}}{10} \tag{12}$$

where h is the characteristic element size, and λ_{min} is the minimum wavelength associated with the highest significant frequency represented in the reconstructed source signature. In

the present model, the actual mesh was non-uniform, and the numerical mesh statistics reported above describe the discretization used in the dynamic analysis. Accordingly, Equation (12) is introduced as a general wave-propagation discretization guideline rather than as a criterion uniformly satisfied throughout the entire computational domain. Because the adopted mesh is strongly non-uniform, the smallest elements are concentrated around the blast-hole and bench regions where the largest dynamic gradients are expected, whereas substantially coarser elements are used in the far field. The reported mesh statistics therefore characterize the actual field-scale numerical discretization rather than a uniformly wavelength-controlled mesh [16,19,21]. Consequently, the present mesh should be interpreted as an engineering-scale discretization optimized for production-blast response simulation rather than as a uniformly dispersion-controlled mesh for the complete high-frequency content of the reconstructed source.

The transient response of the rock mass was solved using the elastodynamic equilibrium equation introduced in Equation (2). In the present formulation, the dynamic excitation term represents the reconstructed equivalent single-hole seismic source signature obtained through the inverse procedure described in Section 2.3, rather than an assumed analytical pressure–time pulse. The reconstructed field-derived excitation was subsequently synchronized with the actual spatial coordinates and electronic initiation times of the production-blast holes.

The rock-mass mechanical properties assigned to the model were derived from the available site-specific characterization. In particular, the value E_{mass} = 0.985 GPa used in the FEM represents the effective rock-mass deformation modulus adopted for field-scale numerical simulation and should not be interpreted as the Young's modulus of intact laboratory rock specimens. This distinction is important because the deformation response of the in situ rock mass reflects the combined influence of intact material, discontinuities, weathering, and field-scale structural compliance. The remaining material and dynamic parameters are summarized in Table 4.

To reduce artificial reflections from the truncated numerical boundaries, Lysmer–Kuhlemeyer viscous boundaries were applied to the external model surfaces. The normal and shear dashpot coefficients are expressed as:

$$c_n = \rho V_p \, \mathrm{A} \tag{13}$$

$$c_s = \rho V_s A \tag{14}$$

where c_n and c_s denote the normal and shear damping coefficients, ρ is the rock density, V_p and V_s are the P-wave and S-wave velocities, respectively, and A is the boundary area associated with each finite element. These absorbing boundaries were used to approximate radiation of seismic energy away from the finite computational domain and to limit spurious wave reflections from the model boundaries.

Time integration was performed using the Newmark-β scheme. The field production-blast initiation sequence lasted approximately 1.8 s and was represented by 137 reported calculation steps. The individual blast holes were activated according to their actual field electronic initiation times rather than by simultaneous or uniformly delayed activation. The complete transient dynamic FEM solution covered approximately 1.8 s, corresponding to the full 0–1799 ms production-blast initiation sequence.

Table 4. Principal geometric, mechanical, dynamic, and numerical parameters used in the three-dimensional dynamic FEM.

Parameter	Value/Description
Computational domain	850 × 460 × 300 m
Number of production blast holes	83
Total number of elements	5581
Total number of nodes	9161
Average element size	52.23 m
Minimum element size	0.9029 m
Maximum element size	128.1 m
Global scale factor	1.2
Minimum element-size factor	0.005
Unit weight, γ	26.80 kN/m^3
Rock-mass deformation modulus, E_{mass}	0.985 GPa
Poisson's ratio, ν	0.25
P-wave velocity, Vp	424 m/s
S-wave velocity, Vs	230.7 m/s
Effective field-scale damping ratio, ξ	3%
Quality factor, Q	70
Dynamic source implementation	Three field-derived equivalent single-hole seismic source histories implemented through component-specific dynamic multiplier functions in PLAXIS 3D
Initiation sequence	Actual field electronic initiation times, applied hole-by-hole
Production-blast initiation duration	≈1.8 s (0–1799 ms)
Total dynamic FEM solution duration	≈1.8 s
Calculation steps	137
Time integration scheme	Newmark-β
Boundary condition	Lysmer–Kuhlemeyer viscous boundaries

The reconstructed equivalent single-hole seismic source signature was synchronized with the actual electronic initiation sequence of the 83-hole production blast, enabling sequential activation of the blast-hole sources according to the measured field timing. The production-blast initiation pattern and individual activation times are presented in Figure 9. This field-derived temporal sequence is distinct from the numerical integration increment: the former defines when each physical source is activated, whereas the latter controls the temporal discretization of the transient numerical solution.

The complete implementation of the three-dimensional dynamic FEM and its integration within the PI-DDT framework is presented in Figure 10, while the principal numerical and field-derived parameters are summarized in Table 4. Within this framework, the FEM constitutes the physics-based computational counterpart of the physical production blast; the broader PI-DDT additionally incorporates field-derived source reconstruction, actual blast geometry and initiation timing, and comparison with measured field responses.

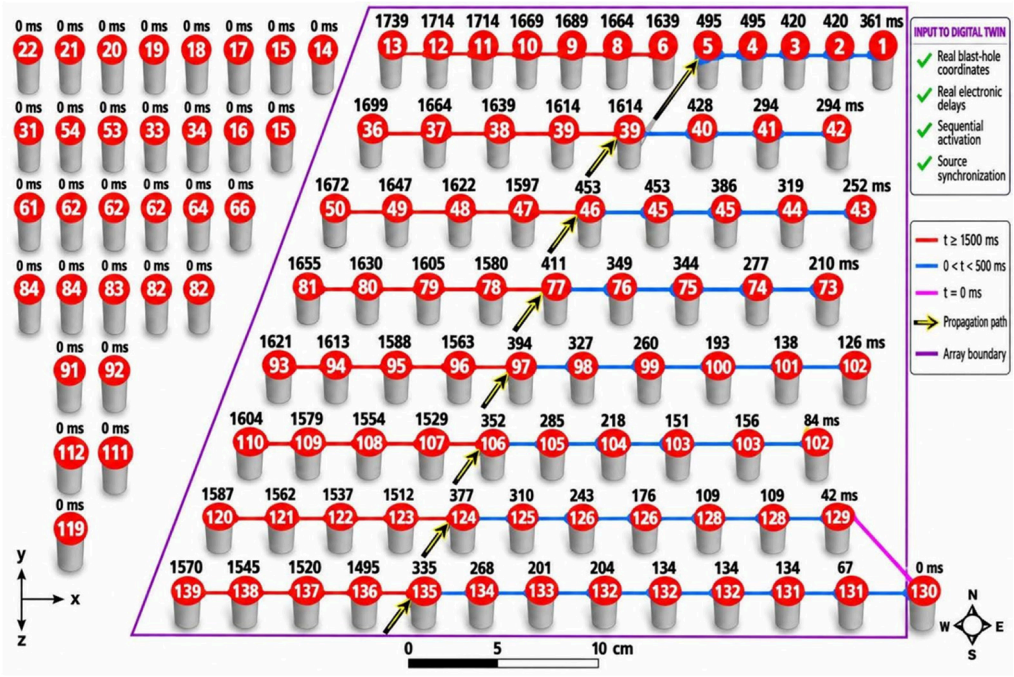


Figure 9. Production blast initiation sequence showing the actual electronic delay timing and sequential blast-hole activation incorporated into the PI-DDT.

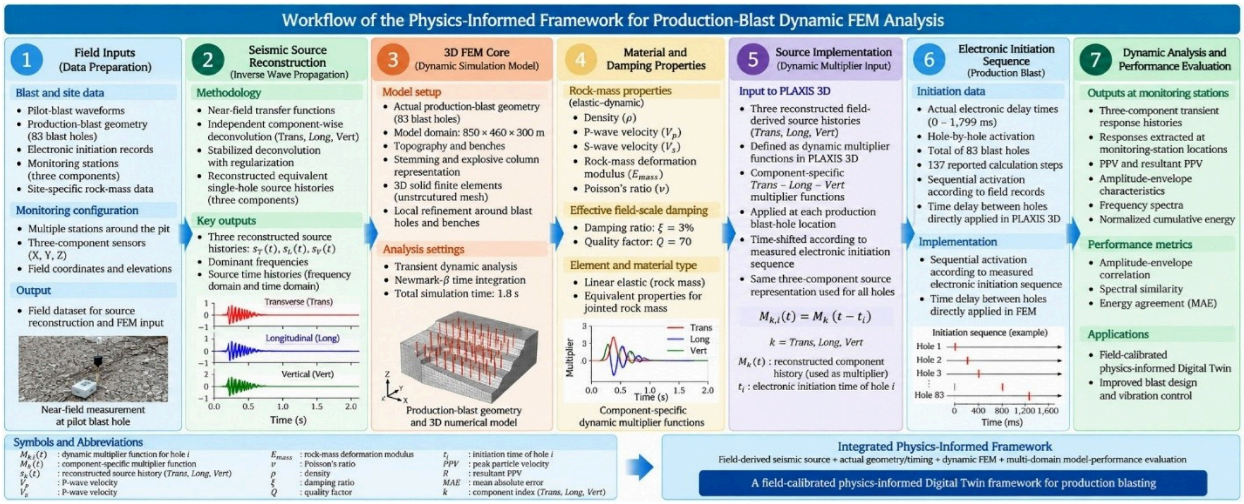


Figure 10. Workflow of the proposed physics-informed framework for production-blast seismic analysis using a three-dimensional dynamic finite element model.

Attenuation and damping in the forward dynamic model were represented using two effective field-scale parameters: the seismic quality factor Q and the damping ratio ξ. These parameters were calibrated at the forward-model stage by iterative comparison of the simulated production-blast responses with the corresponding field-recorded three-component waveforms at the monitoring locations. During calibration, the reconstructed three-component source histories, production-blast geometry, electronic initiation sequence, monitoring coordinates, and rock-mass properties were kept unchanged, while the effective attenuation–damping representation was adjusted to improve the overall field-to-model agreement. The calibration was evaluated jointly in terms of vibration amplitude and attenuation behavior, waveform evolution, and frequency-content preservation rather than by matching PPV alone. The combination Q = 70 and ξ = 3% was retained as the site-specific forward-model calibration set because it provided a practically acceptable simultaneous

representation of vibration amplitude, attenuation behavior, waveform evolution, and frequency content across the available production-blast monitoring records. The calibration was performed as an engineering parameter-adjustment procedure rather than as a formal global optimization; therefore, the selected pair is not claimed to constitute a mathematically unique optimum. Alternative Q–ξ combinations may provide comparable agreement, and systematic joint sensitivity analysis of these parameters is identified as an important requirement for future independent applications of the framework. In this calibration, Q primarily controls the effective attenuation of propagating seismic energy, whereas ξ provides the effective damping representation of the transient FEM response; hence, the two parameters were assessed jointly rather than independently. Because the production-blast records contributed to this calibration, the subsequent comparison between simulated and measured production-blast responses is therefore treated as field-calibrated model-performance evaluation rather than as wholly independent validation.

The resulting model therefore provides a field-calibrated, physics-based computational representation of the investigated production blast. Its role within the proposed PI-DDT is to propagate the reconstructed field-derived source through the actual three-dimensional blast configuration under the measured initiation sequence and site-specific rock-mass conditions. The synchronization procedure linking the reconstructed source, individual blast-hole activation times, and field monitoring locations is described in Section 2.5.

E_{mass} represents the effective rock-mass deformation modulus used in the field-scale numerical model and should not be interpreted as the Young's modulus of intact rock. The proposed framework is not intrinsically restricted to the relatively low rock-mass deformation modulus adopted at the present site. For application to stiffer rock masses with higher E_{mass}, the site-specific stiffness and associated dynamic wave-propagation properties should be re-parameterized using appropriate field and/or laboratory characterization, while the source-reconstruction and field-to-model synchronization procedures remain unchanged. Because increasing rock-mass stiffness can modify wave velocities, impedance, wavelength, and the resulting vibration response, application to substantially higher-modulus rock masses would require site-specific recalibration and independent performance evaluation rather than direct transfer of the present parameter set. The reconstructed source signature was obtained independently from the near-field pilot-blast record as described in Section 2.3. The damping ratio and quality factor were applied during the forward dynamic FEM analysis and were not used in the inverse source-reconstruction procedure.

2.5. Production Blast Digital Twin Synchronization

Following reconstruction of the field-derived seismic source signatures (Section 2.3) and development of the three-dimensional dynamic finite element model (Section 2.4), the physical and numerical descriptions of the production blast were integrated within the proposed Physics-Informed Dynamic Digital Twin (PI-DDT) framework. In the present study, the three-dimensional FEM constitutes the physics-based computational core of the framework; it is not, by itself, considered the Digital Twin. The PI-DDT is established by linking this computational core with the field-derived seismic source, the actual production-blast geometry, the measured electronic initiation sequence, field-calibrated rock-mass parameters, and measured seismic responses. Accordingly, the term Digital Twin is used here to describe a field-calibrated, physics-informed virtual representation of the production-blast process rather than a continuously operating real-time or fully autonomous Digital Twin.

Field-to-model synchronization was implemented using four principal groups of information: (i) the field-derived seismic source histories, (ii) the actual three-dimensional coordinates and geometry of the 83 production blast holes, (iii) the field-recorded electronic

initiation times assigned to the individual holes, and (iv) the rock-mass and dynamic parameters used in the forward FEM analysis. The overall integration pathway is summarized in Figure 10. This formulation preserves both the spatial configuration and the measured temporal structure of the production blast while allowing the dynamic FEM to calculate the resulting wave propagation, interaction, attenuation, and vibration response throughout the computational domain.

The reconstructed three-component source histories were introduced into the PLAXIS 3D model through component-specific dynamic multiplier functions. Separate multiplier histories were defined from the reconstructed transverse (Trans), longitudinal (Long), and vertical (Vert) particle-velocity records and synchronized with the measured electronic initiation time of each production blast hole. This implementation preserved the measured temporal characteristics and relative component amplitudes of the field-derived source histories while allowing the PLAXIS 3D dynamic solver to calculate the corresponding three-dimensional transient response. The transverse (Trans), longitudinal (Long), and vertical (Vert) reconstructed histories were represented as three orthogonal component-specific dynamic multiplier functions. The reconstructed source histories used to define the dynamic multiplier functions were stored at a nominal sampling interval of 0.001 s; only the portion corresponding to the confirmed 1.8 s FEM solution interval was used in the present model-performance evaluation. Thus, the field-derived source was not converted into an assumed nodal force or analytical pressure-time pulse; instead, its measured/reconstructed temporal form was transferred to the PLAXIS 3D model through component-specific dynamic multiplier functions.

The actual electronic initiation sequence incorporated into the model is shown in Figure 9. The 83 blast holes were not activated simultaneously; each hole was activated according to its corresponding field initiation time. The complete production-blast initiation sequence extended from 0 to approximately 1799 ms (≈1.8 s). As described in Section 2.4, the complete 0–1799 ms initiation interval was represented by 137 reported calculation steps over the 1.8 s dynamic FEM solution. Figure 9 therefore represents the field electronic timing sequence imposed on the production-blast model and should not be interpreted as the numerical integration time step of the solver.

For the i-th blast hole, the field-based activation time is expressed as

$$t_i = t_0 + \Delta t_i \tag{15}$$

where t_0 denotes the initiation time of the first blast hole, and Δt_i is the electronic delay assigned to the i-th hole in the field blast. The temporal position of every numerical source activation was therefore inherited directly from the production-blast firing sequence rather than being generated from an idealized simultaneous or uniformly spaced initiation scheme.

Because the reconstructed excitation was implemented through component-specific dynamic multiplier functions, the time-shifted multiplier associated with component k at the i-th blast hole can be written as

$$M_{k,\,i}(t) = M_k(t - t_i) \qquad k \in \{Trans,\ Long,\ Vert\} \tag{16}$$

where $M_{k,i}(t)$ denotes the time-shifted dynamic multiplier function for component k at the i-th blast hole, $M_k(t)$ is the corresponding component-specific dynamic multiplier function defined from the reconstructed source history, and t_i is the measured field activation time of the i-th blast hole. Equation (16) explicitly represents the actual FEM source-loading strategy used in this study. For the complete production blast, the same reconstructed three-component source representation was assigned to the corresponding blast-hole locations,

while the component-specific multiplier functions were shifted in time according to the measured electronic initiation sequence. This procedure preserves the source waveform while reproducing the spatial and temporal progression of the 83-hole blast.

The virtual response was subsequently evaluated at numerical monitoring locations corresponding to the coordinates of the field monitoring stations. Simulated and measured three-component particle-velocity histories were compared at these co-located positions using PPV, amplitude-envelope development, frequency-spectrum similarity, and normalized cumulative-energy evolution. This field-to-model comparison constitutes the performance-evaluation layer of the PI-DDT. Importantly, the production-blast records were also used to calibrate the forward-model attenuation parameters ($Q = 70$ and $\xi = 3\%$); therefore, the subsequent production-blast comparison is treated as model calibration and performance evaluation rather than as wholly independent validation. The source-reconstruction procedure itself remained independent of Q and ξ, as described in Section 2.3.

Within the scope of this study, synchronization is therefore event-based and field-calibrated: the physical blast supplies the source histories, blast geometry, initiation timing, material-calibration information, and monitoring responses, while the numerical counterpart reproduces the corresponding dynamic response. No continuous real-time data assimilation, automatic bidirectional parameter updating, or autonomous control of the physical blasting system was implemented. These capabilities represent future extensions of the proposed framework. This distinction defines the present PI-DDT as a field-calibrated physics-informed Digital Twin framework/prototype and avoids equating the underlying FEM model alone with a fully operational real-time Digital Twin.

3. Results

The performance of the proposed PI-DDT was evaluated by comparing the simulated seismic responses with field measurements obtained during the full-scale production blast. The model-performance evaluation was designed to determine the extent to which the field-calibrated PI-DDT could reproduce the maximum vibration amplitudes together with the principal temporal, spectral, and energetic characteristics of the measured production-blast response. Therefore, model-performance evaluation was performed at multiple monitoring stations using three-component particle-velocity records.

3.1. Production-Blast and Monitoring Configuration

The field-calibrated PI-DDT was evaluated using the full-scale 83-hole production blast and three monitoring stations, UM24232, 12269, and UM6761. The production-blast geometry and monitoring configuration are shown in Figure 11. Quantitative model-performance metrics were calculated directly from the measured and modeled three-component time histories over the complete 0–1.80 s FEM evaluation interval using a sampling interval of 0.001 s.

All quantitative metrics reported below were calculated over the complete 0–1.80 s FEM evaluation interval, corresponding to the full confirmed dynamic solution and electronic initiation sequence. The underlying measured and modeled time histories were sampled at 0.001 s.

3.2. Measured Production-Blast Response

Figure 12 presents the measured transverse, vertical, and longitudinal particle-velocity histories at UM24232, 12269, and UM6761. The records exhibit clear station- and component-dependent differences in peak amplitude, oscillatory structure, and energy development. These differences reflect the combined influence of source–receiver geometry, sequential electronic initiation, attenuation, and local propagation conditions. Because the response

is strongly three-dimensional and oscillatory, model performance was reassessed using several complementary metrics rather than a single PPV value.

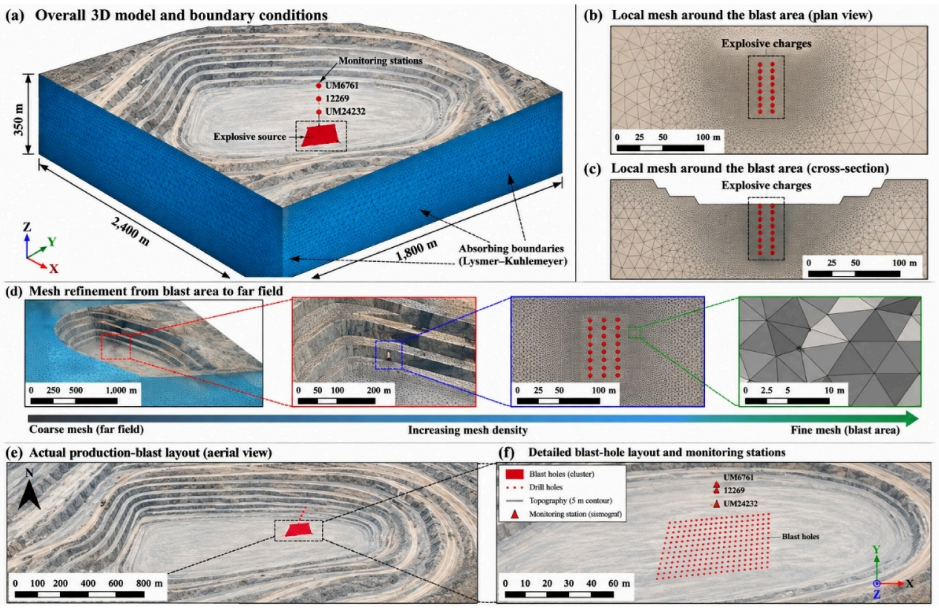


Figure 11. Three-dimensional finite element model geometry and discretization used for the production-blast simulation: (**a**) overall model geometry, dimensions, monitoring-station configuration, and absorbing boundaries; (**b**) plan view of the locally refined mesh around the blast area; (**c**) cross-sectional view of the local mesh refinement around the explosive charges; (**d**) progressive mesh refinement from the far field toward the blast area; (**e**) actual production-blast layout in aerial view; and (**f**) detailed blast-hole and monitoring-station configuration.

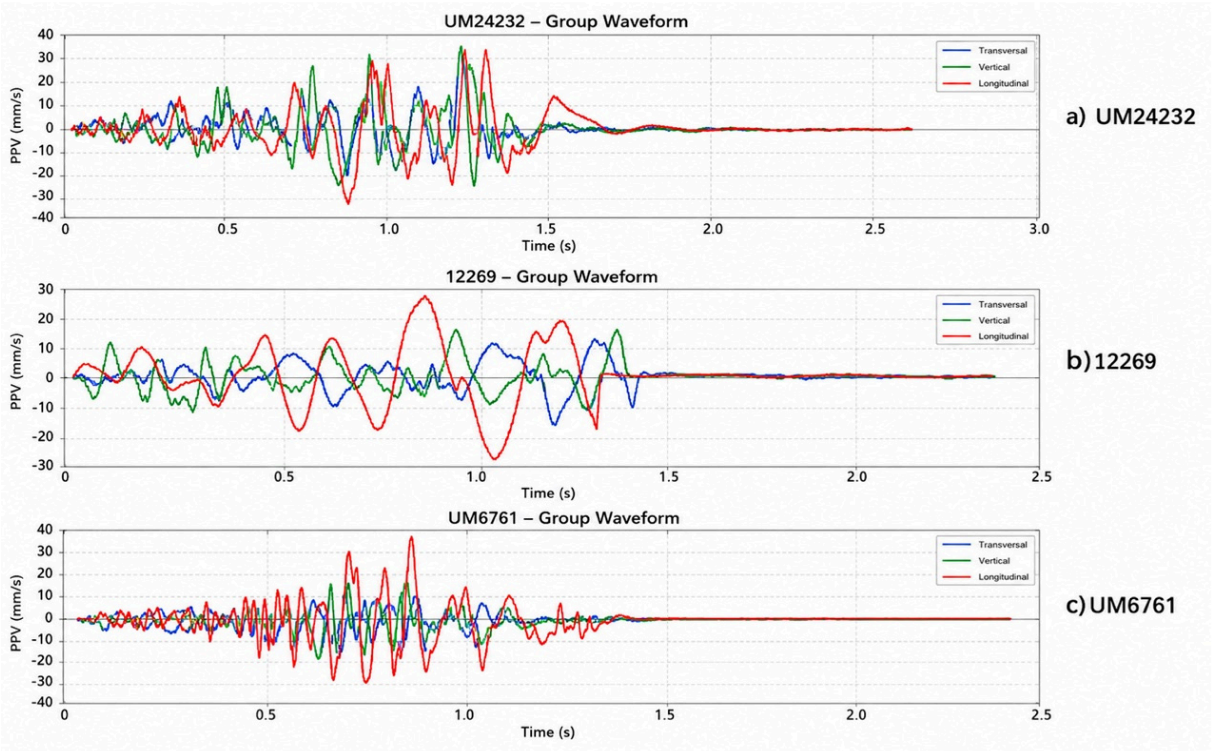


Figure 12. Measured three-component particle-velocity waveforms recorded during the production blast at the three monitoring stations.

Figure 13 presents the time-history comparison between the measured and modeled responses. The quantitative assessment reported below was calculated directly from the underlying numerical time histories rather than from approximate values read from the plotted curves.

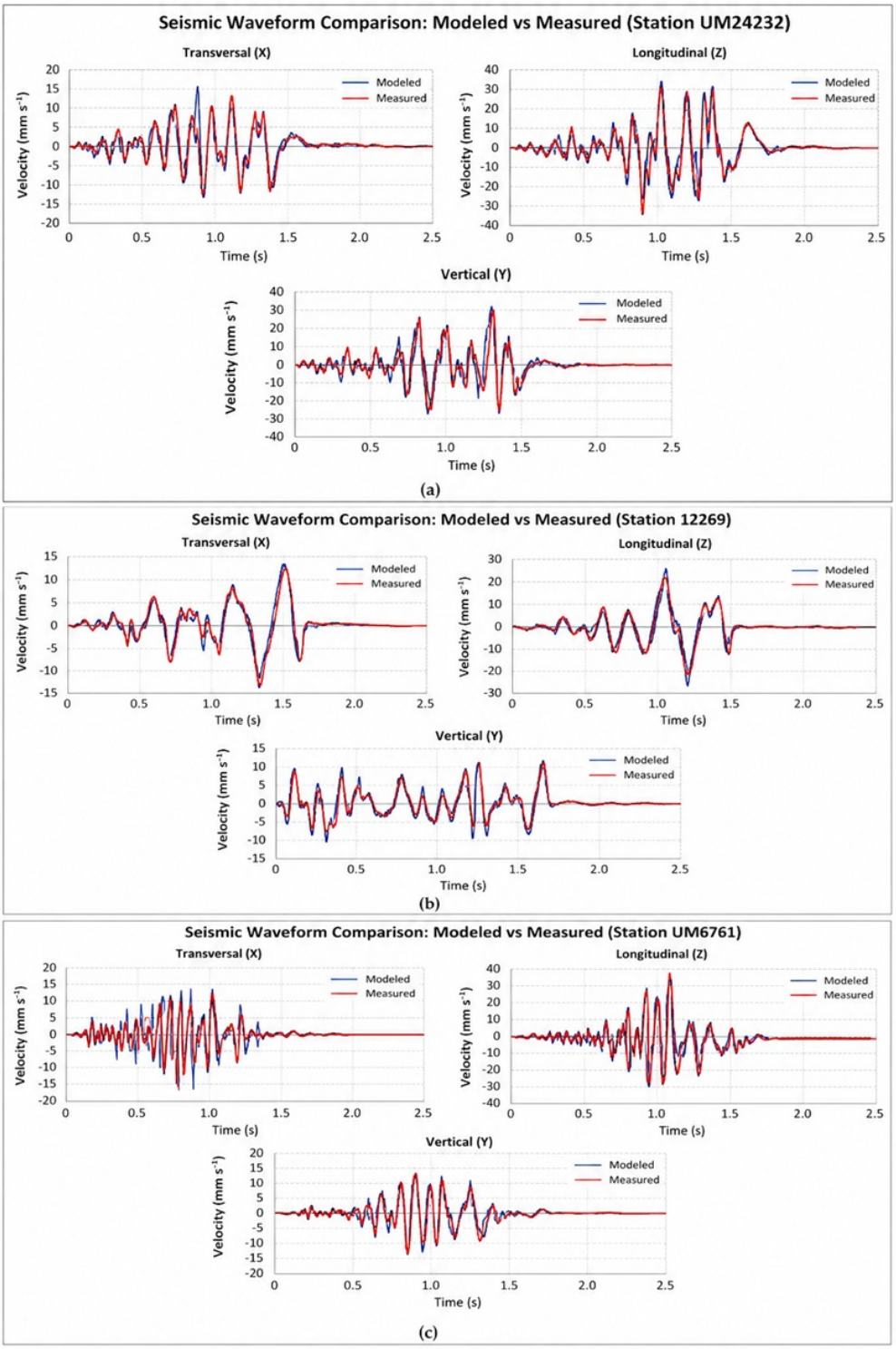


Figure 13. Comparison between measured and simulated three-component particle-velocity waveforms at monitoring stations (**a**) UM24232, (**b**) 12269, and (**c**) UM6761.

As shown in Figure 12, the measured three-component waveforms exhibit distinct amplitudes, waveform morphologies, frequency characteristics, and attenuation behav-

ior at the three monitoring stations owing to differences in propagation distance and wave-propagation paths. These records preserve the complete temporal evolution of the production-blast seismic response and therefore provide substantially more physical information than Peak Particle Velocity (PPV) alone. Consequently, the measured waveforms provide the field reference responses for evaluating the waveform-level performance of the field-calibrated PI-DDT.

3.3. Component-Level Amplitude and Temporal-Envelope Performance

The component-level model-performance metrics are summarized in Table 5. Across the nine station-component combinations, the mean absolute PPV error is 14.86%, and the median is 11.81%. The smallest component error occurs for the UM24232 longitudinal response (1.68%), whereas the largest occurs for the UM6761 transverse response (33.82%). These values provide a component-resolved assessment of amplitude agreement across the three monitoring stations.

Table 5. Component-level multi-domain performance metrics for the measured and modeled production-blast responses over the 0–1.80 s evaluation interval.

Station	Comp.	Measured PPV (mm/s)	Modeled PPV (mm/s)	PPV Error (%)	Envelope r	Spectral Similarity (%)	Energy MAE (%)
UM24232	Trans	17.08	18.68	9.34	0.463	26.31	3.07
UM24232	Long	33.35	33.91	1.68	0.511	35.58	6.60
UM24232	Vert	32.49	34.52	6.26	0.565	63.37	3.08
12269	Trans	12.70	11.20	11.80	0.492	31.48	5.75
12269	Long	27.05	34.43	27.27	0.667	78.78	3.02
12269	Vert	12.57	11.09	11.81	0.355	59.77	6.92
UM6761	Trans	11.48	15.36	33.82	0.682	30.65	3.60
UM6761	Long	33.66	39.53	17.46	0.570	65.90	5.20
UM6761	Vert	15.67	17.91	14.33	0.669	63.04	3.40

Because production-blast records are strongly oscillatory and arise from the superposition of many delayed hole contributions, the temporal comparison was based on the amplitude envelope in addition to peak-amplitude metrics. The mean and median component-level envelope correlations are 0.553 and 0.565, respectively, indicating consistent correspondence in the temporal modulation and development of vibration amplitude. Accordingly, Figure 13 is interpreted primarily in terms of the evolution of the measured and modeled response envelopes, peak amplitudes, and overall dynamic character.

3.4. Frequency- and Energy-Domain Performance

Frequency-domain similarity was calculated from mean-removed, Hann-windowed magnitude spectra over 1–45 Hz. Component-level spectral similarity is variable, with an overall mean of 50.54% and a median of 59.77% (Table 5). The strongest component-level spectral correspondence is obtained for the longitudinal component at station 12269 (78.78%), whereas the transverse components show weaker correspondence. These results indicate that the effective-continuum FEM reproduces the principal spectral characteristics to varying degrees across individual components, while component-wise spectral fidelity remains sensitive to monitoring location and propagation direction.

In contrast, normalized cumulative-energy evolution is reproduced consistently. The mean component cumulative-energy MAE is 4.51%, with a median of 3.60%. Thus, although detailed phase and component-level spectral content are only partially reproduced, the temporal accumulation of vibration energy over the complete blast sequence is captured substantially more robustly. To complement the component-level evaluation, the measured

and modeled responses were further compared using the three-dimensional resultant particle-velocity histories. Figure 14 presents the normalized resultant magnitude spectra and normalized three-dimensional cumulative-energy histories for all three monitoring stations. This representation provides a direct visual assessment of the model performance in both the frequency and energy domains and reduces the influence of directional component partitioning on the comparison.

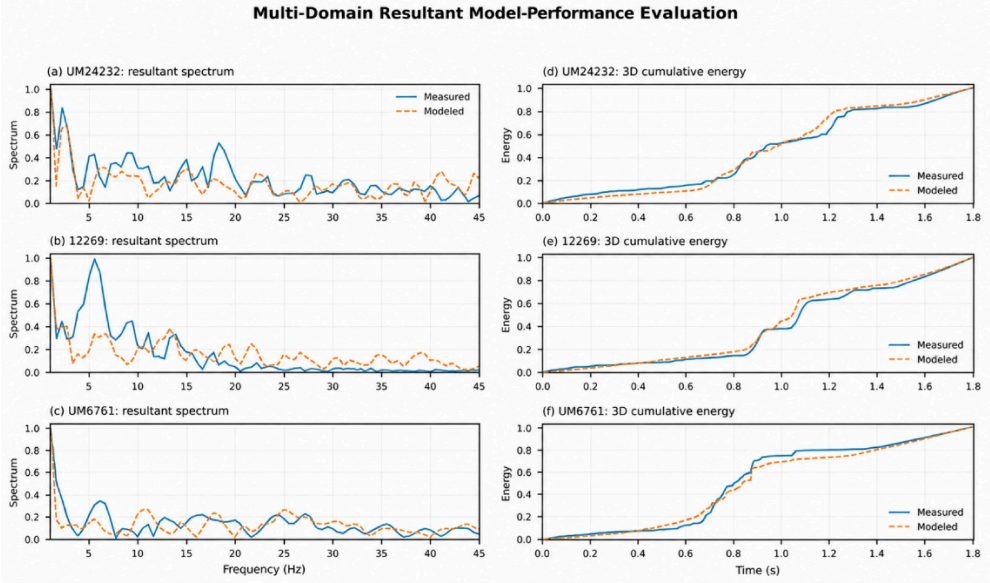


Figure 14. Multi-domain comparison of measured and modeled three-dimensional resultant responses at the three monitoring stations. Normalized resultant magnitude spectra are shown for (**a**) UM24232, (**b**) 12269, and (**c**) UM6761, together with the corresponding normalized three-dimensional cumulative-energy histories for (**d**) UM24232, (**e**) 12269, and (**f**) UM6761. All comparisons were calculated from the measured and modeled response time histories over the complete 0–1.80 s FEM evaluation interval.

3.5. Three-Dimensional Resultant Performance

To reduce sensitivity to component-axis partitioning, the three orthogonal responses were additionally combined into the three-dimensional resultant particle velocity, defined as the Euclidean norm of the transverse, longitudinal, and vertical components at each time step. The corresponding station-level metrics are summarized in Table 6.

Table 6. Station-level three-dimensional resultant model-performance metrics for the measured and modeled production-blast responses.

Station	Mean Comp. PPV Error (%)	Measured Resultant PPV (mm/s)	Modeled Resultant PPV (mm/s)	Resultant PPV Error (%)	Resultant Spectral Similarity (%)	3D Energy MAE (%)
UM24232	5.76	35.99	34.83	3.24	88.57	4.51
12269	16.96	27.97	34.68	23.97	76.53	5.05
UM6761	21.87	34.72	40.06	15.37	86.97	4.67

The resultant PPV errors are 3.24% at UM24232, 23.97% at 12269, and 15.37% at UM6761, giving a station-average resultant PPV error of 14.19%. Importantly, the corresponding resultant spectral similarities are 88.57%, 76.53%, and 86.97%, respectively, while the three-dimensional cumulative-energy MAEs remain between 4.51% and 5.05%.

These results show that the model performs more consistently when evaluated in terms of integrated three-dimensional vibration intensity, spectral content, and energy evolution than when strict component-by-component phase correspondence is required. This distinction is central to the physical interpretation of the PI-DDT performance.

3.6. Overall Model-Performance Synthesis

Taken together, Figures 12–14 and Tables 5 and 6 indicate that the proposed framework reproduces the overall amplitude scale and cumulative energetic development of the production blast with useful engineering fidelity, while exact component-level phase reproduction remains limited. The median component PPV error is 11.81%, the mean three-dimensional resultant PPV error is 14.19%, the mean resultant spectral similarity is 84.02%, and the mean three-dimensional cumulative-energy MAE is 4.74%.

Accordingly, the principal strength of the present PI-DDT lies in its field-based source representation and its ability to reconstruct the global dynamic response across several complementary domains. The multi-domain evaluation therefore emphasizes amplitude, temporal-envelope development, resultant response, spectral content, and cumulative-energy evolution rather than relying on a single waveform-similarity indicator.

4. Discussion

The results presented in Section 3 demonstrate that evaluating a production-blast Digital Twin solely through peak vibration amplitudes provides an incomplete assessment of model performance. Blast-induced seismic waves are inherently transient, multi-component, and frequency-dependent, and therefore their agreement with field observations must be interpreted simultaneously in the amplitude, temporal, spectral, and energy domains. The multi-domain evaluation adopted in this study provides a more comprehensive interpretation of the reconstructed seismic source and its propagation through the three-dimensional rock mass.

Accordingly, this discussion examines the physical significance of the obtained performance metrics rather than considering them as independent statistical indicators. The interpretation focuses on (i) the consistency between measured and simulated responses across complementary performance-evaluation domains, (ii) the influence of station-dependent propagation conditions on model performance, (iii) the implications of the equivalent-continuum FEM assumptions for production-scale blasting, and (iv) the engineering interpretation of the proposed field-calibrated Physics-Informed Digital Twin (PI-DDT) framework.

4.1. Interpretation of the Multi-Domain Model-Performance Evaluation

The quantitative multi-domain evaluation provides a rigorous interpretation of model performance across complementary amplitude, temporal, spectral, and energy domains. The quantitative analysis of the underlying measured and modeled time histories shows that component PPV errors remain moderate overall, while the three-dimensional resultant spectra and normalized cumulative-energy histories exhibit stronger and more spatially consistent agreement.

This pattern demonstrates why a single performance metric is insufficient for evaluating production-blast simulations. PPV evaluates peak amplitude, amplitude-envelope correlation characterizes the temporal modulation of the response, spectral similarity assesses preservation of frequency content, and normalized cumulative energy describes the temporal distribution of vibration energy. Together, these quantities provide a complementary assessment of the global dynamic response.

4.2. Interpretation of Component-Level Temporal and Directional Differences

Blast-induced vibration is a strongly oscillatory response generated by the superposition of many delayed sources. Small differences in local travel time, velocity structure, scattering, and wave-mode conversion can alter individual component phase relationships while preserving comparable amplitude envelopes, spectral characteristics, and cumulative-energy development. The moderate component-level envelope correlations and the stronger resultant spectral and energy-domain performance reported in Tables 5 and 6 are consistent with this behavior.

The effective-continuum FEM does not explicitly represent every discontinuity, heterogeneous propagation path, or local anisotropic feature. The PI-DDT should therefore be interpreted as a field-calibrated physics-informed representation of the production-blast response whose principal performance strength lies in the combined reproduction of peak amplitude, temporal-envelope evolution, resultant response, spectral content, and cumulative energy.

4.3. Station Dependence of Model Performance

The station-level results in Table 6 demonstrate that predictive fidelity varies spatially. UM24232 exhibits the strongest resultant PPV agreement, with an error of only 3.24%. UM6761 exhibits strong resultant spectral similarity (86.97%), although its resultant PPV is overpredicted by 15.37%. Station 12269 shows the largest resultant PPV error (23.97%) and the lowest resultant spectral similarity (76.53%), while its three-dimensional energy evolution remains well reproduced (MAE = 5.05%).

The higher measured longitudinal and vertical PPV values at UM6761 than at the closer station 12269 demonstrate that vibration amplitude is not controlled by source–receiver distance alone; directional wave propagation, local discontinuity geometry, topographic effects, and component-dependent wave-mode contributions can produce non-monotonic spatial variations in the measured response. Although UM6761 is located farther from the blast area (34 m) than station 12269 (28 m), its measured longitudinal and vertical PPVs are higher. This non-monotonic distance–amplitude relationship is physically plausible because blast-induced vibration is not governed by source–receiver distance alone. Component-specific amplitudes are also affected by source–receiver orientation, local topography, discontinuity-controlled propagation, wave-mode conversion, and constructive or destructive superposition of the sequentially delayed blast-hole contributions. Consequently, a farther monitoring point may exhibit a larger directional PPV than a closer point when the corresponding propagation path and component orientation are more favorable for energy transmission. This spatial variability is physically reasonable for a rock mass represented by effective continuum properties. Different source–receiver paths may sample different discontinuity sets, attenuation characteristics, local topography, and anisotropic wave-propagation conditions. The observed station dependence therefore provides an important indication of where additional spatially resolved characterization would be required to improve future PI-DDT implementations.

4.4. Implications for Attenuation and Damping Calibration

The forward model uses globally calibrated attenuation and damping parameters. The present results indicate that such parameters can reproduce the overall energetic behavior of the blast but cannot guarantee identical performance along every propagation path or for every directional component. In this sense, Q and damping should be interpreted as effective field-scale parameters rather than unique intrinsic constants of the entire rock mass.

The adopted values Q = 70 and ξ = 3% should therefore be interpreted in the context of the present calibration event. Their purpose is to provide an effective field-scale representation of attenuation and damping within the investigated production-blast configuration, rather than to imply a unique constitutive characterization of the rock mass. The station-dependent differences observed in the multi-domain performance metrics further indicate that a single global Q–ξ representation cannot fully capture spatially variable propagation effects.

Future studies should investigate spatially variable attenuation, direction-dependent damping, and explicit representation of dominant discontinuity systems where sufficient site data are available. Such extensions are particularly relevant for improving phase and component-level spectral fidelity without compromising the present framework's direct linkage to field-derived source information.

4.5. Digital Twin Interpretation

The results also clarify the appropriate use of the Digital Twin terminology. The three-dimensional FEM is the physics-based computational core, while the PI-DDT framework results from coupling this core with the reconstructed field source, actual blast-hole geometry, measured electronic initiation sequence, field-calibrated material and attenuation parameters, and production-blast monitoring data. The present implementation is therefore best described as a field-calibrated physics-informed Digital Twin framework or prototype rather than a continuously operating real-time Digital Twin.

The multi-domain results support the usefulness of this framework for scenario analysis and physics-based blast-response assessment. Continuous data assimilation, automated state updating, uncertainty quantification, and spatially variable propagation properties remain important future developments before the framework can be regarded as a continuously operating predictive Digital Twin.

4.6. Calibration Versus Independent Validation

A further methodological distinction is necessary when interpreting the production-blast comparison. The field-derived source reconstruction is independent of the forward-model attenuation and damping calibration. However, because production-blast observations contributed to the selection of Q and damping parameters, the final production comparison should not be described as wholly independent validation. Accordingly, the production-blast comparison is interpreted here as a field-calibrated model-performance evaluation rather than as wholly independent validation.

The next stage of validation should apply the calibrated framework without parameter retuning to one or more additional production blasts. Such blind or hold-out applications would provide a stronger test of predictive generalization and would allow the Digital Twin concept to be evaluated beyond the calibration event.

4.7. Limitations and Future Development

The present study has four principal limitations. First, the rock mass is represented by effective continuum properties and does not explicitly resolve all joints, weak zones, or anisotropic propagation paths. Second, the reconstructed seismic input is an equivalent field-derived source representation rather than a direct simulation of detonation, near-hole crushing, and gas-driven fracture development. Third, the attenuation and damping parameters are globally calibrated. Fourth, the current PI-DDT is event-based and does not yet include continuous field-data assimilation or autonomous bidirectional updating.

Future work should therefore focus on independent validation using additional production blasts, spatially variable attenuation and anisotropy, uncertainty propagation, and sequential updating of the virtual model using new monitoring data. These developments

would improve spatial and component-level predictive performance while retaining the principal advantage of the present approach: the direct integration of field-derived source information with a three-dimensional physics-based production-blast model.

5. Conclusions

This study developed a field-calibrated Physics-Informed Dynamic Digital Twin (PI-DDT) framework for production blasting by integrating field-derived seismic source reconstruction, three-dimensional dynamic finite element modeling, actual blast-hole geometry, real electronic initiation timing, site-specific rock-mass properties, and measured production-blast responses within a unified computational workflow.

The central methodological contribution of the framework is the replacement of idealized analytical blast-loading functions with an equivalent seismic source reconstructed from pilot-blast field measurements through deconvolution-based inverse wave propagation. The reconstructed three-component source histories were subsequently introduced into the PLAXIS 3D model through component-specific dynamic multiplier functions and propagated through the actual 83-hole production-blast configuration.

Performance evaluation using the production-blast monitoring records demonstrated that the proposed framework reproduced the overall vibration magnitude, spectral characteristics, and temporal energy development with practically meaningful agreement. Across the three monitoring stations and nine component responses, the median component PPV error was approximately 11.8%, while the mean component PPV error was approximately 14.9%. The mean error in the three-dimensional resultant PPV was approximately 14.2%. At the same time, the mean three-dimensional resultant spectral similarity was approximately 84.0%, and the mean three-dimensional cumulative-energy MAE was approximately 4.7%. These results indicate that the PI-DDT captures the principal amplitude, frequency, and energy characteristics of the production-blast response, although component-level waveform fidelity remains sensitive to local propagation conditions.

The results also demonstrate the importance of evaluating blast-response models using multiple physical domains rather than PPV alone. The combined assessment of amplitude, spectral similarity, envelope evolution, and cumulative-energy development provides a more complete and physically informative measure of model performance.

The present implementation should therefore be interpreted as a field-calibrated, event-based PI-DDT framework or prototype rather than a continuously operating real-time Digital Twin. The dynamic FEM constitutes the physics-based computational core, whereas the Digital Twin functionality arises from its integration with field-derived source information, actual production-blast geometry and timing, calibrated dynamic properties, and measured response data.

The production-blast records were also used in the calibration of the effective attenuation and damping representation. Accordingly, the reported comparison represents a field-calibrated model-performance evaluation rather than a wholly independent validation. Future work should therefore focus on independent testing using additional production blasts, spatially and directionally variable attenuation, improved representation of structural anisotropy and discontinuity-controlled wave propagation, automated model updating, uncertainty quantification, and continuous sensor-driven data assimilation.

Within these limitations, the proposed PI-DDT provides a physically grounded framework for moving blast-vibration assessment beyond conventional empirical PPV prediction toward field-informed numerical replication. It offers a promising basis for future applications in blast-design evaluation, vibration-control planning, scenario analysis, and progressively more adaptive Digital Twin implementations in mining and blasting engineering.

Supplementary Materials: The following supporting information can be downloaded at: https://www.mdpi.com/article/10.3390/mining6040085/s1, Supplementary Sections S1–S4, Section S1, Regularization-Parameter Sensitivity; Section S2, FEM Configuration and Component-Wise Source Implementation; Section S3, Detailed Multi-Domain Model-Performance Metrics; Section S4, Three-Dimensional Resultant Performance.

Author Contributions: C.O.A.: conceptualization; development of the Physics-Informed Dynamic Digital Twin (PI-DDT) framework; methodology; seismic source reconstruction methodology; blast-engineering interpretation; finite-element modeling strategy; formal analysis; model-performance evaluation methodology; interpretation of field and numerical results; supervision; project administration; writing—original draft preparation; writing—review and editing. G.G.U.A.: methodology; development of the physics-informed modeling framework; formal analysis; interpretation of numerical and field results; scientific evaluation of the Digital Twin methodology; validation; writing—review and editing. H.E.Y.: dynamic finite-element modeling; numerical model implementation; seismic-response analysis; processing and evaluation of measured and modeled waveforms; quantitative model-performance analysis; data analysis; visualization; software; writing—review and editing. V.O.: field investigation; production-blast monitoring; blast-design and field-data evaluation; interpretation of geological and rock-mass conditions; validation of field observations; technical review; writing—review and editing. O.S.: field-data acquisition and processing; production-blast data organization; electronic initiation-sequence implementation; seismic-data processing; numerical-model data preparation; data curation; quantitative analysis; visualization; software support. All authors have read and agreed to the published version of the manuscript.

Funding: This research received no external funding.

Data Availability Statement: The data supporting the findings of this study are not publicly available due to confidentiality restrictions and data-ownership agreements associated with the industrial mining operation. The authors do not have authorization to distribute the field and operational data directly. For scientifically justified requests, access to the relevant data may be considered subject to prior approval and permission from the data-owning company. Interested researchers may contact the corresponding author, who may facilitate a formal data-access request to the company; however, data availability cannot be guaranteed and will remain subject to the company's authorization and applicable confidentiality requirements.

Conflicts of Interest: Ozan Savas is affiliated with GOA Mining Co. The remaining authors declare no conflicts of interest. GOA Mining Co. had no role in the interpretation of the results or in the decision to publish the manuscript.

References

1. Siskind, D.E.; Stagg, M.S.; Kopp, J.W.; Dowding, C.H. *Structure Response and Damage Produced by Ground Vibration from Surface Mine Blasting*; U.S. Bureau of Mines Report of Investigations 8507; U.S. Bureau of Mines: Washington, DC, USA, 1980.
2. Dowding, C.H. *Construction Vibrations*; Prentice Hall: Upper Saddle River, NJ, USA, 1996.
3. Langefors, U.; Kihlström, B. *The Modern Technique of Rock Blasting*, 3rd ed.; John Wiley & Sons: New York, NY, USA, 1978.
4. Persson, P.A.; Holmberg, R.; Lee, J. *Rock Blasting and Explosives Engineering*; CRC Press: Boca Raton, FL, USA, 1994.
5. Konya, C.J.; Walter, E.J. *Surface Blast Design*; Prentice Hall: Englewood Cliffs, NJ, USA, 1990.
6. Khandelwal, M.; Singh, T.N. Prediction of blast-induced ground vibration using artificial neural network. *Int. J. Rock Mech. Min. Sci.* **2009**, *46*, 1214–1222. [CrossRef]
7. Monjezi, M.; Ghafurikalajahi, M.; Bahrami, A. Prediction of blast-induced ground vibration using artificial neural networks. *Tunn. Undergr. Space Technol.* **2013**, *33*, 30–37.
8. Hasanipanah, M.; Monjezi, M.; Shahnazar, A.; Jahed Armaghani, D.; Farazmand, A. Feasibility of indirect determination of blast induced ground vibration based on support vector machine. *Measurement* **2015**, *75*, 289–297. [CrossRef]
9. Armaghani, D.J.; Hajihassani, M.; Mohamad, E.T.; Marto, A.; Noorani, S.A. Blasting-induced flyrock and ground vibration prediction through an expert artificial neural network based on particle swarm optimization. *Arab. J. Geosci.* **2015**, *8*, 5383–5396. [CrossRef]
10. Koopialipoor, M.; Jahed Armaghani, D.; Haghighi, M.; Ghaleini, E.N. A neuro-genetic predictive model to approximate overbreak induced by drilling and blasting operation in tunnels. *Bull. Eng. Geol. Environ.* **2019**, *78*, 981–990. [CrossRef]

11. Zhou, J.; Asteris, P.G.; Armaghani, D.J.; Pham, B.T. Prediction of ground vibration induced by blasting operations through the use of the Bayesian network and random forest models. *Soil Dyn. Earthq. Eng.* **2020**, *139*, 106390. [CrossRef]
12. Sanchidrián, J.A.; Segarra, P.; López, L.M. Energy components in rock blasting. *Int. J. Rock Mech. Min. Sci.* **2007**, *44*, 130–147. [CrossRef]
13. Ouchterlony, F.; Nyberg, U.; Olsson, M.; Bergqvist, I.; Granlund, L.; Grind, H. Where does the explosive energy in rock blasting rounds go? In Proceedings of the 30th Annual Conference on Explosives and Blasting Technique, New Orleans, LA, USA, 1–4 February 2004.
14. Aldaş, G.G.U.; Ecevitoğlu, B.; Kaypak, B.; Can, A.; Toprak, B.; Babayiğit, E.; Erguder, İ.; Kaçan, M. Partition of plastic/elastic energy in mine blasts. In *Proceedings of the 22nd International Mining Congress of Turkey, Ankara, Türkiye, 11–13 May 2011*; Chamber of Mining Engineers of Turkey: Ankara, Turkey, 2011; pp. 117–126.
15. Uyar, G.G.; Aksoy, C.O.; Ecevitoğlu, B.; Kaypak, B. Partition of Plastic/Elastic Energy in Mine Blasts. In *Proceedings of the International Conference on Mining, Material and Metallurgical Engineering (MMME'14), Prague, Czech Republic, 11–12 August 2014*; Paper No. 146; International ASET Inc.: Ottawa, ON, Canada, 2014.
16. Lysmer, J.; Kuhlemeyer, R.L. Finite dynamic model for infinite media. *J. Eng. Mech. Div.* **1969**, *95*, 859–877. [CrossRef]
17. Aki, K.; Richards, P.G. *Quantitative Seismology*, 2nd ed.; University Science Books: Sausalito, CA, USA, 2002.
18. Zienkiewicz, O.C.; Taylor, R.L.; Zhu, J.Z. *The Finite Element Method: Its Basis and Fundamentals*, 6th ed.; Elsevier Butterworth-Heinemann: Oxford, UK, 2005.
19. Hughes, T.J.R. *The Finite Element Method: Linear Static and Dynamic Finite Element Analysis*; Dover Publications: Mineola, NY, USA, 2012.
20. Belytschko, T.; Liu, W.K.; Moran, B.; Elkhodary, K.I. *Nonlinear Finite Elements for Continua and Structures*, 2nd ed.; Wiley: Chichester, UK, 2014.
21. Bathe, K.J. *Finite Element Procedures*, 2nd ed.; Klaus-Jürgen Bathe: Watertown, MA, USA, 2016.
22. Uyar Aldaş, G.G.; Ecevitoğlu, B. Waveform analysis in mitigation of blast-induced vibrations. *J. Appl. Geophys.* **2008**, *66*, 25–30. [CrossRef]
23. Uyar Aldaş, G.G.; Ecevitoğlu, B.; Can, A.Z. Application of surface wave mitigation method in minimizing blast-induced vibration: A practice at TKİ YLİ Milas Enterprise. *Ank. Univ. J. Environ. Sci.* **2009**, *1*, 83–93. [CrossRef]
24. Uyar Aldaş, G.G. Investigation of blast design parameters from the point of seismic signals. *Int. J. Min. Reclam. Environ.* **2010**, *24*, 80–90. [CrossRef]
25. Uyar Aksoy, G.G.; Aksoy, C.O. Comparative review and interpretation of the conventional and new methods in blast vibration analyses. *Geomech. Eng.* **2019**, *18*, 545–554.
26. Uyar Aksoy, G.G.; Aksoy, C.O. Seisblast_Plus: The First National Software in the World to Design Surface Blast with Seismic Wave Analysis. In *Proceedings of the 28th International Mining Congress and Exhibition of Türkiye (IMCET 2023), Antalya, Türkiye, 28 November–1 December 2023*; UCTEA Chamber of Mining Engineers: Antalya, Türkiye, 2023; pp. 302–309.
27. Grieves, M. *Digital Twin: Manufacturing Excellence through Virtual Factory Replication*; White Paper; Florida Institute of Technology: Melbourne, FL, USA, 2014.
28. Glaessgen, E.; Stargel, D. The digital twin paradigm for future NASA and U.S. Air Force vehicles. In Proceedings of the 53rd AIAA/ASME/ASCE/AHS/ASC Structures, Structural Dynamics and Materials Conference, Honolulu, HI, USA, 13–26 April 2012.
29. Tao, F.; Zhang, H.; Liu, A.; Nee, A.Y.C. Digital Twin in industry: State-of-the-art. *IEEE Trans. Ind. Inform.* **2019**, *15*, 2405–2415. [CrossRef]
30. Fuller, A.; Fan, Z.; Day, C.; Barlow, C. Digital Twin: Enabling technologies, challenges and open research. *IEEE Access* **2020**, *8*, 108952–108971. [CrossRef]
31. Jones, D.; Snider, C.; Nassehi, A.; Yon, J.; Hicks, B. Characterising the Digital Twin: A systematic literature review. *CIRP J. Manuf. Sci. Technol.* **2020**, *29*, 36–52. [CrossRef]
32. Rasheed, A.; San, O.; Kvamsdal, T. Digital Twin: Values, challenges and enablers from a modeling perspective. *IEEE Access* **2020**, *8*, 21980–22012. [CrossRef]

Disclaimer/Publisher's Note: The statements, opinions and data contained in all publications are solely those of the individual author(s) and contributor(s) and not of MDPI and/or the editor(s). MDPI and/or the editor(s) disclaim responsibility for any injury to people or property resulting from any ideas, methods, instructions or products referred to in the content.